Centrifugal Compressor Stall Control by the Application of Engineered Roughness on Diffuser Shroud

By

Amjid Khan
Reg # 00000205922
Session 2017-2020

Supervised by
Dr. Adeel Javed

A Thesis Submitted to the US Pakistan Centre for Advanced Studies in Energy in partial fulfillment of the requirements of the degree of

MASTER of SCIENCE
in
THERMAL ENERGY ENGINEERING

US-Pakistan Centre for Advanced Studies in Energy (USPCAS-E)
National University of Sciences and Technology (NUST) H-12, Islamabad 44000, Pakistan

July, 2020

THESIS ACCEPTANCE CERTIFICATE

Certified that final copy of MS/MPhil thesis written by Amjid Khan (Registration No. 00000205922), of U.S.-Pakistan Centre for Advanced Studies in Energy has been vetted by undersigned, found complete in all respects as per NUST Statues/Regulations, is within the similarity indices limit and accepted as partial fulfillment for the award of MS/MPhil degree. It is further certified that necessary amendments as pointed out by GEC members of the scholar have also been incorporated in the said thesis.

Signature: _____

Name of Supervisor: Dr. Adeel Javed

Date: _____

Signature (HoD): _____

Date: _____

Signature (Dean/Principal): _____

Date: _____

Certificate

This is to certify that work in this thesis has been carried out by **Mr. Amjid Khan** and completed under my supervision in, US-Pakistan Center for Advanced Studies in Energy (USPCAS-E), National University of Sciences and Technology, H-12, Islamabad, Pakistan.

Supervisor: _____

Dr. Adeel Javed
USPCAS-E
NUST, Islamabad

GEC member # 1: _____

Dr. Majid Ali
USPCAS-E
NUST, Islamabad

GEC member # 2: _____

Dr. Adeel Waqas
USPCAS-E
NUST, Islamabad

GEC member # 3: _____

Dr. Mariam Mehmood
USPCAS-E
NUST, Islamabad

HoD-Thermal Energy Engineering: _____

Dr. Adeel Javed
USPCAS-E
NUST, Islamabad

Principal/ Dean: _____

Dr. Adeel Waqas
USPCAS-E
NUST, Islamabad

List of Publications

1. Amjid Khan, Adeel Javed "Performance Variation of Transonic Centrifugal compressor at Different Tip Clearances Using Numerical Simulations" 6th International Conference on Aerospace Science and Technology, November 2019, Institute of Space Technology, Islamabad, Pakistan

Acknowledgment

I would like to take some time at the end of this thesis to thank all the individuals without whom this project was never feasible. Although it's just my name on the cover, many individuals have contributed in their own manner to the studies and I thank them for that.

My supervisor, Dr. Adeel Javed, you developed an invaluable room for me to do this study in the best possible manner and to develop myself as a researcher. I substantially appreciate the liberty you gave me to discover my own route and the advice and help you gave me when it was necessary. Your friendly guidance and professional advice were invaluable throughout all the work phases.

I would also like to take a moment to thank Dr. Majid Ali, Dr. Adeel Waqas, and Dr. Mariam Mahmood, members of the GEC Committee. I am proud and honored that you accepted my committee's presence.

Dedication

I dedicate my thesis to my parents for their support through out my educational career and giving me the strength to chase my dreams.

Abstract

Automotive turbochargers consist of two parts; turbine and compressor, Centrifugal compressor is the fundamental part. Downsizing in the engine size is pushing the automotive industry to operate the compressor at a low mass flow rate. However, the operation of the turbocharger centrifugal compressor at a low mass flow rate leads to fluid flow instabilities. These flow instabilities are flow separation and flow recirculation and because of these instabilities, compressor enters the state of the stall and/or surge. To reduce or eliminate these flow instabilities is the focus of turbomachinery aerodynamics and this research. In the current study, surface roughness has been applied on diffuser shroud, as a passive flow control method to reduce the compressor flow instabilities and increase the stall margin and operating range of the centrifugal compressor for the applications of automotive turbochargers.

The analysis is carried out using a baseline SRV2-O compressor developed and fabricated by the German Aerospace Center named DLR. The steady-state analysis is carried out in two parts. In the first part, detailed aerodynamics of centrifugal compressor has been performed. Numerical simulations have been performed to validate the experimental data by comparing it with the data obtained from the numerical simulations and performance has been evaluated over a constant rotational speed from stall to choke using both k-ε and k-ω SST turbulence models. In the second part, the application of roughness as a passive flow control method on the diffuser shroud and overall performance has been simulated for different roughness heights from stall to choke using both turbulence models. After the application of surface roughness, a significant reduction in flow instabilities has been observed. The results obtained from this analysis showed significant enhancement inflow structure of the diffuser as flow separation and flow reversal has been reduced.

Keywords: Centrifugal compressor, surface roughness, numerical simulations, flow instability, stall margin

Table of Contents

List of Figures

List of Tables

Nomenclature

Variables		Abbreviations	
ε	Epsilon	CFD	Computational Fluid Dynamics
η	Efficiency	DLR	German Aerospace Center
μ	Kinematic Viscosity	SM	Stall Margin
υ	Dynamic Viscosity	SST	Shear Stress Transport
ρ	Density	TE	Trailing-Edge
$\bar{u}_i$	Fluctuating Velocity	LE	Leading Edge
u_i	Mean Velocity	2D	Two Dimensional
K_s	Sand Grain Diameter	3D	Three Dimensional
K^+	Dimensionless sand grain parameter	RANS	Reynolds Average Navier Stokes
π	Total Pressure Ratio	USAID	United States International Development Agency
β	Inlet Flow Angle		
k	Kinetic Energy		
l^*	Length Scale		
U	Free stream velocity		
ω	Specific Rate of Dissipation		
y+	Near Wall Grid Spacing		
C_p	Specific Heat Constant		
τ	Wall Shear Stress		
Re	Reynolds Number		
y_+	Non-dimensional wall distance		
$Re_{\theta t}$	Transition onset momentum thickness Reynolds number		

Chapter 1

Introduction

1.1 Motivation

The centrifugal compressor stability is limited at low mass flow rate by the stall and/or surge. These flow instabilities cause the deterioration of the compressor at a low mass flow rate and should be eliminated. As the centrifugal compressor is used in automotive turbocharger specifically, therefore elimination of flow instabilities is very important. Engine downsizing helps in fuel economy and emission reduction but compensates for performance loss. At low mass flow rate large separations occur near the diffuser shroud and result in performance instability and ultimately lead to surge. These flow instabilities cause noise, extremely high blades vibratory stresses and performance loss of the compressor. Hence it is extremely important to develop a method to postpone flow separation and reduce/eliminate these flow instabilities. The current study mainly focuses on surface roughness installation on diffuser shroud to reduce flow separation inside the centrifugal compressor.

These flow instabilities begin due to stall at a low mass flow rate. Stall is a phenomenon, which occurs because of flow separation of flow from the boundary walls. The flow near the wall delays and then it does not follow the wall anymore, due to which streamlines near the wall leave the wall and wake develop there along the surface. The adverse pressure-gradient and viscous shear stress along the wall overcome the momentum of the flow and force the flow to deviate from the wall which induces flow reversal and hence stall phenomenon occurs. The following topics give the literature review of centrifugal compressor operation and flow instabilities i.e. stall and surge.

1.2 Operation and Performance

The impeller is the rotating part of the centrifugal compressor covered with the stationary casing, used to give high velocity to air, which enters the eye of the impeller, rotated at high speed by the vanes on the impeller disc. An impeller is several fixed diverging passages in which air is decelerated with a consequent rise in static pressure and these diverging passages are known as diffusers. Diffusion can be explained by Bernoulli's principle which states that the sum of kinetic energy, potential energy, and pressure head is constant. So, in a diffuser either vaned or vaneless the flow decelerates and increases the potential energy and pressure. In impeller at any point in airflow, the centripetal force is obtained by pressure head, and this static pressure rise from the eye to the impeller tip, and the rest of the impeller pressure is a rise in a diffuser but it causes stagnation pressure loss because of friction loss in a diffuser. The design requirement is that half the pressure rise in the impeller and the rest in the diffuser. Compared to the trailing face, static pressure rise is greater on forward face. The air that flows between impeller and casing results in loss of efficiency, which means that clearance should be as small as possible but small clearance also results in windage loss. Increasing static pressure at a low mass flow rate is the most important purpose of a centrifugal compressor.

Fluid radially flows outward from the eye of the impeller to discharge it into the static component of the centrifugal compressor, called the diffuser. As the fluid travels through the rotating component called a rotor, energy is transmitted to the fluid particles. A portion of the energy is directly converted to pressure while another part is transformed into kinetic energy. As the fluid enters the diffuser section, the kinetic energy of the fluid decreases which results in the augmentation of the static pressure rise. The increase in pressure in rotor section is a consequence of the backward sweep of the blades. To get high-pressure conversion in the impeller, keep the blades less radial[3]. When the blades are less radial and more curled, then because of centrifugal forces pressure rise is restricted by the mechanical stresses arises in the impeller. That's why centrifugal compressors have a higher operating range and it is also desired in a centrifugal compressor to have a high operating range and small flow instabilities.

To show the performance Speedline of the compressor, a performance map between pressure ratio and mass flow rate at constant rotational speed from stall to choke for the test case compressor has been presented [4].

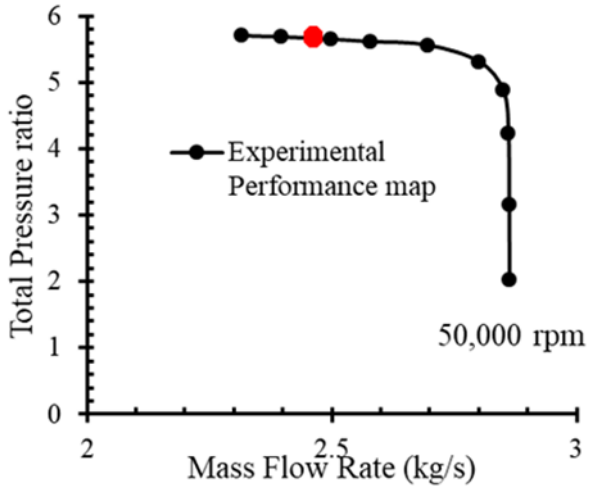

Figure 1: Performance Map of Test Case Compressor

1.3 Flow Instabilities

The applications of high-pressure ratio centrifugal compressors are micro gas-turbines and turbos of the vehicles. For high-pressure rise across the impeller, splitter blades are used with unshrouded impellers. Consequently, due to tip-leakage between shroud casing and blade tip of the compressor stage, losses in the pressure ratio results in the degradation of the performance. These losses lead to flow instabilities in the centrifugal compressor [1]. These flow instabilities mostly occur at a low mass flow rate leading to surge, rotating stall at unsteady state analysis. Consequences of these flow instabilities have a great impact on the performance, i.e. pressure ratio and Isentropic efficiency. There are 3 main operating points in the operation of a centrifugal compressor, stall point, design point, and choke point. The flow instabilities that occur in Centrifugal compressor are at stall point (low mass flow rate), which leads to flow separation, flow recirculation, and adverse pressure gradient. The test case SRV2-O compressor used in this analysis is designed and manufactured by the German aerospace center (DLR). In turbocharged applications, the operation of the centrifugal compressor at a low mass flow rate is the most important point to work on

to control flow instabilities. The automotive turbocharger compact size demand leads to fuel economy and emission reduction, but this feature compensates in the form of performance loss. Compressor blades have high vibratory stresses operating at a low mass flow rate because of stall and/or surge. Hence it is mandatory to reduce flow instabilities and augment the stall margin of the centrifugal compressor [2]. The present study emphasizes the effects of roughness on the performance of the centrifugal compressor.

The choke limit is reached at maximum mass flow rates due to the occurrence of sonic conditions in the throat of the rotor. Any attempt to raise the flow rate beyond this limit will result in an increased shock strength, thus effectively reducing the compressor efficiency. As the flow rate through the system is reduced to small values, strong fluctuations and limit cycle oscillations are observed. This limit is called the *surge limit* and is also referred to as a *stall line* or *instability limit* [3]. Two types of flow phenomena, *rotating stall* and *surge*, give rise to the surge limit. Near the surge limit, fluctuations can grow in amplitude and cause considerable fatigue and damage to the entire compression system. If the fluctuations are left unchecked, even a complete flow reversal is possible, a situation that an engine cannot tolerate since hot combustion products would damage the compressor blades and lead to a catastrophic failure of the entire system. Modern centrifugal compressors with vaneless diffusers and pressure ratios between three and five achieve a stable flow rate range of 30 to 40 percent based on the maximum flow rate [4].

1.3.1 Stall

The stall is the flow instability phenomena that occur at low mass flow rates and results in the flow separation from its path of flow [5]. Flow along the surface of the wall may reduce its speed/ momentum and separates from the wall that it may no longer attach to the wall. As this flow leaves the wall, the reverse flow starts to occur near the surface of the wall due to the adverse pressure gradient. In this way, the viscous shear stresses and adverse pressure gradient overcome the momentum of the flow [6], [7]. When this phenomenon happens then the flow leaves the boundary wall and the flow is then called stalled flow. When stall phenomena happen in one or multiple components of

the compressor, then this is said to be stage stalled. In the case of our analysis, the diffuser shroud flow separation leads to stall at the diffuser section, that is why it is called stage stall. In the case of stall phenomena flow separation leads to flow instabilities.

1.3.2 Compressor Steady stall

Flow separation and flow reversal due to the adverse pressure gradient on the diffuser shroud surface causes the phenomena of the stall. A steady stall can occur in two forms singular separation and 3D separation. The flow reversal due to adverse pressure gradient causes singular separation in the fluid flow [2]. The streamlines near the boundary surface of diffuser separate from the diffuser shroud and due to adverse pressure gradient, vortex/wake form near the surface. The occurrence of secondary flow causes ordinary separation or 3D separation. The primary flow of the compressor usually follows the cross-channel flow pattern, when this primary flow is superimposed by minor flow because of the pressure gradient in the channel, then this minor flow is called secondary flow. This flow is different in both speed and direction from the flow pattern of primary flow [8][2].

Ordinary separation occurs in the case of a vaneless centrifugal compressor, where the flow streamlines have a sharp tangential velocity component, but radial velocity component reduces significantly in magnitude. Due to adverse pressure gradient the fluid flow reverses back towards the trailing edge of the blade and hence the condition of the reverse flow occurs.

1.3.3 Inducer Stall and Recirculation

The impeller inlet velocity triangle is illustrated in Fig. 2. At reduced mass flow rate and constant rotational speed, inlet flow angle increases, which results in augment in incidence angle. This incidence angle causes the flow to increase its speed at the leading edge of the blade. This flow causes immense diffusion in the flow to delay flow separation because minor flow separates from the primary flow and hence the streamlines do not follow the surface/ wall of the compressor. According to Japikse, due to the high incidence angle this immense diffusion causes flow separation.

1.3.4 Impeller Stall

Boundary layer development starts across the suction surface of the impeller blade and diffuser shroud, when the flow enters the impeller passage. This flow forms a very complex flow pattern when both core flow and boundary layers advance through the impeller flow path [1]. The Coriolis force field or cross passage force field is experienced by flow, when it enters the eye of the impeller and changes its direction from axial to the radial direction within the impeller flow field. Coriolis force is the apparent force that as a result of impeller rotation forces moving fluid to the exit of the impeller in a direction perpendicular to the direction of motion and rotation and the effect produced by Coriolis force is called Coriolis effect [9]. The Coriolis force may be written as:

$$F_C = 2m(\Omega \times V_\perp) \qquad (1)$$

As equation 1. Indicates that the dependency of the Coriolis force is on the velocity of the fluid particles and rotational speed of fluid element and its purpose is to separate the low-velocity streamlines from high-velocity streamlined elements. As it separates the low-velocity streamlines from the core flow, it results in secondary flow with low speed and low momentum that surrounds the core flow near the shroud surface of the impeller, whereas high-speed fluid is stick to the hub of the impeller pressure surface [4]. Besides these robust Coriolis forces leads to skewed boundary layers and these layers are expected to leave the impeller flow path [1]. Furthermore, the pattern of the impeller flow is also greatly affected by the tip leakage flow.

1.3.5 Diffuser Stall

The diffuser can be subjected to stall that may be a singular or three dimensional in addition to rotating stall [2]. The flow reversal due to adverse pressure gradient causes singular separation in the fluid flow. The ordinary or three-dimensional stall is very common which is attributed to the secondary flow at the diffuser shroud which occurs due to pressure gradient in the cross-channel direction in centrifugal compressor. While singular stall rarely occurs in the diffuser section. The evaluation of diffuser performance is based on the following equations:

$$rVt = constant \quad (2)$$

$$\rho . V_m . 2\pi rb = m \quad (3)$$

$$\tan \alpha = \frac{V_t}{V_m} \quad (4)$$

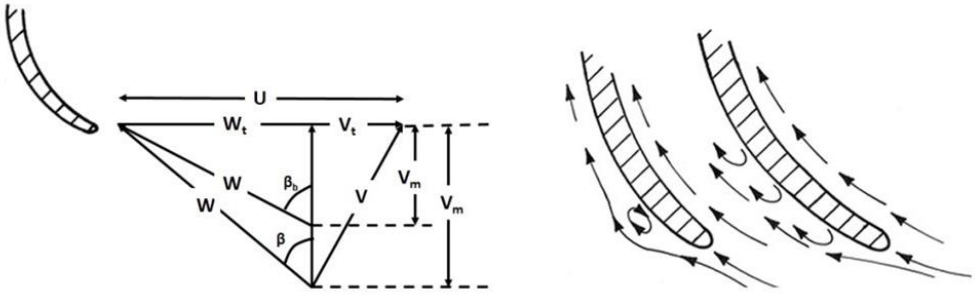

Figure 2: Impeller Inlet velocity triangle

The conservation of mass and momentum is shown by the above-mentioned equations through the vaneless diffuser. It can be perceived from the above equation that the flow angle is dependent on the density of the flow and depth of the passage. Thus, at the design mass flow rate, a constant flow angle means that constant density has been assumed. The through-flow component tends to follow spiral. However, the flow near the surface of the diffuser shroud has low kinetic energy, which means that at the same radial pressure gradient the meridional velocity at the shroud of the diffuser is lower. Hence it doesn't follow the constant flow angle and hence separates from the surface [10].

1.3.6 Dynamic Stall and Surge

Two types of unsteady flow phenomenon occur when the mass flow rate is dropped in the compressor [11]:

- **Rotating Stall:**
  Rotating stall is a flow phenomenon in which uniform flow pattern along the circumference is distributed by local flow separation [12]. At low mass flow rates, due to a high incidence angle, local flow separation occurs at the leading edge of the compressor blades due to non-uniform inflow conditions and system perturbations [13]–[15]. This results in a partial blockage of the stalled

flow passage, which leads to a deflection of the incoming flow. While one flow Passage experiences a smaller incidence angle which results in the flow re-attachment locally, the inflow conditions for other flow Passage produce separation. As a result, local separation packets transfer from one blade to another, and at angular velocity these packets rotate around the shaft of the impeller, which is 1.5 times the shaft angular velocity. In most of cases the rotating stall is the precursor of the surge phenomena, but this kind of instability does not affect the flow pattern of the compressor. The important differentiation between rotating stall and surge is that during surge the mean flow is unsteady while in case of rotating stall the mean flow is steady with a rotating mass discrepancy. Rotating stall phenomena have been measured in many axial compressors. Periodic blade loadings with oscillations near resonance frequencies can cause blade damage or even blade fracture. Centrifugal compressor is desired for high-pressure systems at a low mass flow rate at partial speed. The heavily used centrifugal compressor configurations for high-pressure systems in industries, the rotating stall has a very small effect on pressure ratio and mass flow rate and very rarely leads to surge [16].

- **Surge:**

  The other form of flow instability of unsteady nature that occurs as an effect of the decrease in mass flow rate is called surge [17]. Surge consist of large periodic fluctuations in the flow rate and pressure develops as the system operates at conditions near or beyond the surge line. This results in the fluctuations in the mass flow rate at the diffuser cross-section. Fluid compressibility represents the potential energy, and the inertia of the particles is the kinetic energy. Limit-cycle oscillations due to surge occur at frequencies that are equivalent or below the natural system frequencies [5], [18], [19]. Depending on the severity of the flow fluctuations there are three types of surge mild surge, classic, modified and deep surge [3]. Mild and classic surge operates at medium rotor speed and there is no flow reversal in this case [20]. Whereas periodic pressure fluctuations are more severe in the case of classic as compared to mild surge. Blend of the rotating stall and classic stall is called

a modified surge [21]. When the classic surge becomes extremely intense, then it is named as deep surge and operates at high rotor speeds involves strong flow reversal [22].

1.4 Boundary layer and flow separation transition

As discussed in the previous section 1-2, that the primary contributor in the flow instabilities is the flow separation along the wall of the diffuser shroud surface of the compressor. In this part of the chapter, the flow separation, and boundary layer transition has been described on the walls of the compressor.

The basic phenomenon responsible for the flow separation, flow departure or flow breakaway is the excessive momentum loss near the diffuser shroud due to adverse pressure-gradient against the streamlines, the flow separation appear to start between low and high-velocity flow elements, $\frac{dp}{dx} > o$.

The terminology transition means the change in the boundary layer state from laminar to turbulent. The main factors that affect or delay the transition process are unsteady passing of wakes and free-stream turbulence, adverse pressure gradient, vortex generators, and surface roughness [23]. Mayle studied the different types of flow and laminar to turbulent flow transition phenomena and its effect on the aerodynamics and heat transfer of the modern turbine engines and he concluded that the effects of adverse pressure gradient, surface roughness and unsteady passing of wakes and free-stream turbulence on transition are secondary to those of free-stream turbulence. Mayle also studied the transition phenomena in gas turbine airfoils and he implied that transition phenomena in these airfoils are the multi moded type which suggests that at the same time transition can occur at two locations on the same surface and this transition can occur on the surface of laminar separation bubbles, fluctuating turbulent spots and the whole surface can be affected by the passing of reverse flow-induced transition repeatedly. Schlichting experimentally investigated the rough surface effect on turbulent flow and during his analysis he made few assumptions that have a significant effect on turbulent flow transition [24]. If the transition is divided into different modes, then it has three modes: natural transition; bypass transition; separated flow transition.

The turbulence that appears in the free streamlines of the flow and minor flow instability in the laminar boundary layer cause natural transition. High freestream turbulence results in bypass transition and when the laminar boundary layer separates due to adverse pressure gradient then the transition mode is separated flow transition. Due to these transitions a laminar transition bubble appears at a point between separation and reattachment point at the surface. The flow separation, flow reversal, or recirculating flow regions that occur as a result of adverse pressure gradient causes hostile effects such as augment in drag and vibrations of the blades and all these discrepancies occur at low mass flow rate [25].

1.5 Transition Modelling and Computational Fluid Dynamics

Most of the commercial 3D solvers have been modelled using different algorithms to study laminar flow and turbulent flow structure in many industrial applications. The computational power of new ultra-fast computing facilities made it extremely economical for numerical fluid dynamics analysis of the real-world applications. The experimental cost has been reduced by selecting most optimum structural and aerodynamics design using numerical simulations. For this purpose, many solvers have been developed time to time i.e. VISIUN, STAGE3D, TASCFlow, and FLOWSIM. All these solvers provided very realistic results for all the radial flow machinery specifically for centrifugal compressor. Though most of these solvers have not incorporated to evaluate the transition from laminar-turbulent very well and due to which different transition model predicts extremely different results that are commercially available to study turbulent flows [26].

Most compatible formulations with CFD methods are low Reynolds number models. The lowest closure level where the actual instability is simulated is the e^n method, these transitions simulations are based on the linear stability analysis. As the n-factor depends on the free stream environment and wind tunnel, hence this factor is not universal and that's why the e^n method has also practical applications. One of the main difficulties is using e^n model is that structure needed for this model is very complex. Velocity profiles are mainly used in stability analysis, which is derived from extremely resolved boundary layer codes, these profiles are then coupled with the RANS solver

for the pressure distribution. The stability method then takes the output from the boundary layer method and provides this information back to the turbulence model in the RANS solver. This model is mainly used in applications, the flow is supposed to be close to stability limit for drag force reduction such as the laminar airplane wing design, where the complexity of this model is justified [27].

The most suitable tools for transition prediction are DNS and LES, even though, the appropriate condition of the external disturbance level and structure poses substantial challenges. These numerical methods are too much expensive for engineering applications and are presently used for research applications and used to eliminate the need for controlled experiments.

In the present study, a different turbulence model (k-ε and k-ω SST model) has been used. These turbulence models are present within the commercial software package ANSYS CFX [2].

1.6 Boundary-Layer Transition, Surface Roughness, and Applicability to Turbomachinery

Boundary layer transition from laminar to turbulent is one of the important factors in reducing flow separation at high Reynolds number. There are many techniques to reduce flow separation, which occurs due to adverse pressure gradient and results in the aerodynamic efficiency losses in turbomachinery. These techniques are Surface Roughness, application of vortex generators on the fluid surface, or creating a cavity for flow separations. Surface roughness is one of the most effective passive flow control methods with a low reduction in performance. This method is used in many engineering applications where there are flow separation and backflow conditions. For example, in heat exchangers and Scramjet, it is employed to increase heat transfer rates and mixing. All those cases where laminar flow separation is tripping, tripping a transition from laminar to turbulent is preferable and desired by creating vortices and keeping the flow stick to the surface or delaying flow separation as a result of high momentum [23]. At low Reynolds number, there are no vortices/wakes and at high Reynolds number, this surface roughness effect is used to increase the speed of transition from laminar-turbulent [28].

For early laminar-turbulent transition, surface roughness is applied on the surface of the compressor walls to avoid Laminar flow separation on aerodynamic surfaces. This separation in centrifugal compressor occurs, as a result, an adverse pressure gradient, which results in the decrease of aerodynamic efficiencies and pressure ratio of the compressor due to increased pressure drag. In turbomachinery, where there is laminar flow separation occurs, due to the addition of surface roughness, flow separation delays. Local flow separations in the flow structure occur at the rough surfaces. Wake regions which are comprised of counter rotating vortex pairs initiating on rough surface [28]. Based on length scale of the wake roughness element size is presented that cause flow separation from the diffuser shroud. Now a sublayer induced by surface roughness near the wall of the compressor mixes into the flow. As mentioned above the low Reynolds number flow suppress the vortices/wakes with the help of viscosity but at high Reynolds number these wakes speed up the transition process from laminar to turbulent. Surface roughness affects both the compressors and turbines. Based on the general trends it is still beyond our ability to predict the roughness effects on losses due to fluid friction and surface heat transfer accurately. There is still a very large gap in research to properly characterize roughness e.g. size, shape, spacing, and blade location. Equivalent sand grain roughness characterization (k_s) has impeded comprehensive use for modeling since it doesn't account for different roughness effects on heat transfer, skin friction, and boundary layer transition [28].

Nikurasde closely investigated the effect of roughness on different surfaces on the turbulent flow structure. The dependencies of different flow regions on Reynolds number and different surface roughness was obtained from the Nikurasde pressure loss data. Nikurasde in his study on surface roughness, based on the diameter of sand grain (K_S), dynamic viscosity (υ), and wall friction velocity (V^*) he defined a dimensionless parameter $K^+ = (K_s V^*)/ \upsilon$. The loss coefficient is only a function of k_s and 70 is defined value for this parameter. The parameters Re and K^+ become too much important when the value of k_s is between 5 and 70. Nikurasde defined three different regions based on his analysis:

- Hydraulically smooth region ($0 < K^+ < 5$), in this region the size of the grain is too small that it has no significant impact on the performance of the compressor
- Transition region ($5 < K^+ < 70$), in this region the sand grain/roughness elements are great enough to project out of closest layer to wall and further resistance is observed because of high surface roughness
- Completely Rough region ($K^+ > 70$), in this region all the sand grain/roughness heights is greater than the length scale of viscous sublayer and drag form of opposition is offered

To elaborate the further concept of sand grain roughness has been further formulated by Schlichting. He used the concept of equivalent sand grain roughness for converting the roughness data and measurement equivalent to the roughness data used by Nikurasde corresponding to several more flow profiles into roughness profiles [28]. Improved and advance corrections to the concept of Schlichting were provided by Colman *et al. and* further these correlations were developed by Simpson.

1.7 Objectives

This study is carried out to achieve the following objectives:

- To control stall phenomena using engineered surface roughness as a passive flow control method
- To increase the operating range of the SRV2-O compressor
- To draw performance map at constant speed for different mass flow rates

This baseline compressor used in this study is SRV2-O compressor developed by DLR (German Aerospace Center). In this research, surface roughness has been introduced as a passive flow control method on diffuser shroud to control stall phenomena. In the first phase of the study, the validation of experimental data of the SRV2-O compressor has been carried out using ANSYS-CFX. The methodology for the validation case is given below stepwise:

- 3D model in BLADEGEN

- Mesh in TURBOGRID
- Simulations in ANSYS-CFX module

The performance output parameters for the validation case is total pressure ratio and isentropic efficiency. Moving on to the second phase after the validation case, roughness has been introduced as a passive flow control method for stall control. The stepwise methodology for design optimization after application of surface roughness on the diffuser surface is as follows:

- Roughness on Diffuser shroud in ANSYS CFX Pre Processing
- Simulations
- Design Optimization for Stall control in ANSYS CFX post-processing

To study the steady-state simulations, the following research methodology has been executed using the CFD ANSYS CFX module for numerical simulations. The flow chart diagram for the methodology is shown in Fig. 1.

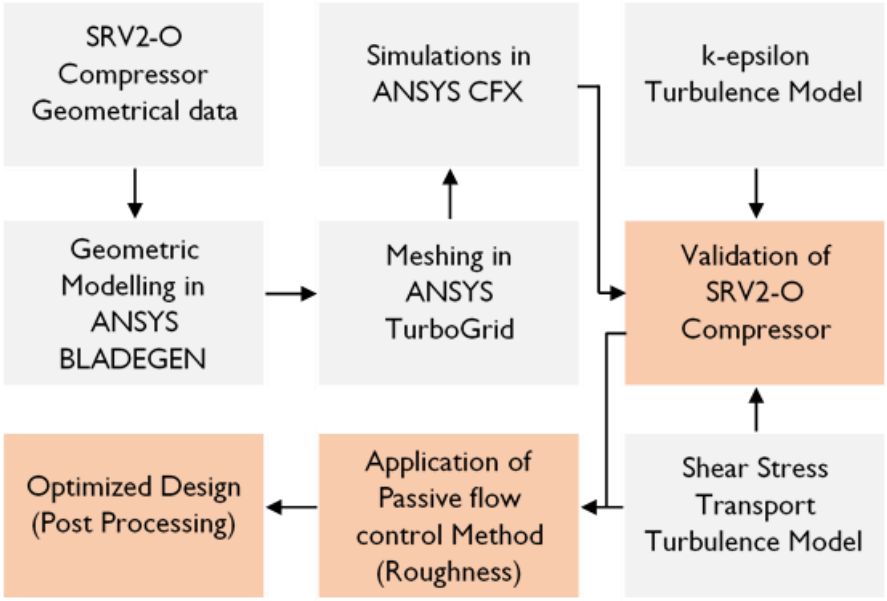

Figure 3: Flow Sheet Diagram of Methodology

1.8 Outlines of the Thesis Report

Chapter 2 presents the literature review about the numerical modeling, the concept, and equations behind the turbulence models (k-ε and k-ω SST models), the transition from laminar to turbulent flow by the application of surface roughness, the influence of the roughness height on the performance of the compressor. This chapter also presents the equations Reynolds averaged Navier-Stokes equations and the concept behind these equations.

Chapter 3 presents setup made for the numerical simulations and computational analysis using ANSYS-CFX to study the aerodynamics of centrifugal compressor. Moreover, this chapter provides an overview of the validation of experimental data and the initiation of the flow instabilities and flow separation locations.

Chapter 4 presents the influence of roughness heights on the performance of the compressor and how it reduces the flow separation across the compressor instable locations. It also gives brief insights about the difference between both the turbulence models (k-ε and k-ω SST models).

Chapter 5 explains the conclusion and also defines the future recommendations for the improvement in this research.

Chapter 2

Literature Review

This chapter reviews the literature and theoretical background of the centrifugal compressor for the laminar-turbulent transition and turbulence modeling, and surface roughness effect on the performance of turbomachinery. A short explanation of turbulence models (K-ε) and (K-ω SST) have been given in section 2.1. Further a study has been carried out on the boundary layer transition and the numerical concept is presented in section 2.2. Section 2.3 of this chapter deals with the influence of surface roughness on the performance of turbomachinery and specifically the centrifugal compressor performance degradation with the application of passive flow control method (surface roughness).

2.1 Numerical Modelling

Numerical methods are defined by John D. Anderson as:

"*CFD is the skill, which replaces the governing partial differential equations of fluid flow with numbers and then these numbers in space and/or time is used to get the whole flow field of the analysis. The final result of CFD is just a combination of numbers.* [29]*"*

This part of the chapter presents the governing equations of the with numerical approximation according to the current research. The fluid motion can be completely described by the partial differential equations for the conservation of mass, energy, and momentum in fluid flows. These equations are combinedly referred to as Navier-Stokes equations. These equations describe continuum fluid flow, which is explained by the classic work of Schlichting [24]. Considered Continuum, meaning that flow quantities such as pressure and temperature are approximately uniform within fluid elements [30]. The set of equations is known as the compressible Navier Stokes equations:

Continuity equation [31]:

$$\frac{\partial u}{\partial x} + \frac{\partial v}{\partial y} + \frac{\partial w}{\partial z} = 0 \qquad (5)$$

Momentum Equation [31]:

In the x-direction,

$$u\frac{\partial u}{\partial x} + v\frac{\partial u}{\partial y} + w\frac{\partial u}{\partial z} = -\frac{1}{\rho_f}\frac{\partial p}{\partial x} + \frac{\mu_f}{\rho_f}\left(\frac{\partial^2 u}{\partial x^2} + \frac{\partial^2 u}{\partial y^2} + \frac{\partial^2 u}{\partial z^2}\right) \qquad (6)$$

In the y-direction,

$$u\frac{\partial v}{\partial x} + v\frac{\partial v}{\partial y} + w\frac{\partial v}{\partial z} = -\frac{1}{\rho_f}\frac{\partial p}{\partial y} + \frac{\mu_f}{\rho_f}\left(\frac{\partial^2 v}{\partial x^2} + \frac{\partial^2 v}{\partial y^2} + \frac{\partial^2 v}{\partial z^2}\right) \qquad (7)$$

In the z-direction,

$$u\frac{\partial w}{\partial x} + v\frac{\partial w}{\partial y} + w\frac{\partial w}{\partial z} = -\frac{1}{\rho_f}\frac{\partial p}{\partial z} + \frac{\mu_f}{\rho_f}\left(\frac{\partial^2 w}{\partial x^2} + \frac{\partial^2 w}{\partial y^2} + \frac{\partial^2 w}{\partial z^2}\right) \qquad (8)$$

where μ_f and ρ_f are dynamic viscosity and density of the working fluid, respectively. Note, that p stands for pressure, and v stands for velocity of the fluid.

Energy Equation [31]:

$$u\frac{\partial T_f}{\partial x} + v\frac{\partial T_f}{\partial y} + w\frac{\partial T_f}{\partial z} = \frac{k_f}{\rho_f C_{pf}}\frac{\partial p}{\partial z} + \left(\frac{\partial^2 T_f}{\partial x^2} + \frac{\partial^2 T_f}{\partial y^2} + \frac{\partial^2 T_f}{\partial z^2}\right) \qquad (9)$$

Where T_f, k_f, and C_{pf} are the temperature, thermal conductivity, and constant specific heat capacity of the working fluid.

The equation (5) presents the conservation of mass, while the equation (6-9) represents the momentum conservation of the fluid volume. It is very difficult to calculate the approximation and tenacity of all sizes of turbulent flows, irrespective of the accessibility of complex and commanding computational facilities. The only solution to the above problem is Reynolds-averaged Navier-Stokes equations. The Reynolds breakdown is the basis for the RANS equations, this equation includes the breakdown of a small instantaneous quantity into mean and variating parts. After the complete

breakdown of the RANS model, the velocity u and pressure *p* at each instant can be written as:

$$u_i = \bar{u}_i + \acute{u} \qquad p_i = p + \acute{p} \tag{10}$$

where, u_i stands for mean velocity, $\bar{u}_i$ stands for fluctuating velocity, p_i stands for mean pressure and *p* stands for variation in pressure. Replacing the mentioned breakdown in the RANS equation which results in the following equations:

$$\frac{\partial}{\partial xi}\,(\bar{u}_i + \acute{u}) = 0 \tag{11}$$

$$\frac{\partial}{\partial t}(\bar{u}i + \acute{u}i) + (\bar{u}j + \acute{u}j)\frac{\partial}{\partial xj}(\bar{u}i + \acute{u}i) = -\frac{1}{\rho}\frac{\partial}{\partial x}(p + \acute{p}) + v\frac{\partial^2}{\partial x^2}(\bar{u}i + \acute{u}i) \tag{12}$$

After applying the RANS model breakdown, which is followed by statistical averaging to equation 13 and 14, the above equation results in:

$$\frac{\partial \bar{u}i}{\partial xi} = 0 \tag{13}$$

$$\frac{\partial \bar{u}i}{\partial t} + \bar{u}i\frac{\partial \bar{u}i}{\partial xj} = -\frac{1}{\rho}\frac{\partial p}{\partial x} + v\frac{\partial^2 ui}{\partial x^2} + \frac{\partial ui * uj}{\partial xj} \tag{14}$$

The equations mentioned above are referred to as RANS Equation. Equation 14 is the original RANS equation but with the addition of one more term and this additional last term is used for Reynolds stress. The four governing equations for numerically 3D flow that regulate involve velocity field, these equations are elements of the RANS equation and accompanied by continuity equation. This set of four equations has more than four unknowns. There are Reynolds stresses besides *u* and *p*. when there are more unknowns than the number of equations, then such a set of equations are called unclosed. These equations form the closure problem of RANS equations i.e. these equations need to solve and determine the Reynolds stresses somehow. The term Reynolds stress comes from the flow and length scales of deviations. Due to perturbations it is not possible to presume a constant number for all instances and therefore it is important to be designed precisely. For this problem to solve, the Boussinesq proposed hypothesis for turbulent viscosity is used [32]. The hypothesis

proposed by Boussinesq narrates the deviatoric Reynold's stress to the average flowrate.

$$\acute{u}i\ \acute{u}j = \frac{2}{3}k + vt(\frac{\partial \bar{u}i}{\partial xj} + \frac{\partial \bar{u}j}{\partial xi}) \quad (15)$$

where *vt* stands for turbulent viscosity and *k* stands for the kinetic energy. If the proper specification of the turbulent viscosity (*vt*) is calculated, then the above equation (15) gives closure to the Reynolds equations (14). Additionally, the turbulent viscosity (*vt*) can be stated as the cross product of the velocity scale and length scale, according to the given equation:

$$Vt = u^{*}l^{*} \quad (16)$$

Where u^{*} stands for velocity scale and l^{*} stands for the length scale.

As different turbulence models represent the turbulence viscosity in different forms and ways. The velocity scale and length scale can be assumed to give a proper estimate of turbulent viscosity. For example, the length scale is assumed based on the geometry of the flow in the case of the mixing length model. However, the velocity and length scale are related to the dissipation rate (ε) and turbulence kinetic energy (*k*) for which the equations are solved in the case of the *k*-ε model.

In the present study *k*-ε and SST turbulence models are applied for analysis. This numerical algorithm is explained in the next portion.

2.1.1 Shear Stress Transport Turbulence-Model

The SST model given by Mentor [32], is an eddy viscosity turbulence model that effectively combines the *k*-ω and *k*-ε model, studying the boundary viscous sublayer using the *k*-ω model of Wilcox and switches to *k*-ε model in the outer region and free shear layers. This model is formed by the multiplication of the mixing of these two models and then sum together. When studying near the boundary layer then this model converts to *k*-ω model, the mixing function assumes a value of one. This turbulence model applies the *k*-ε model when it studies the flow far from the boundary wall, it takes zero a value of the mixing function. Additionally, at low Reynolds number the turbulent viscosity term is neglected from the SST turbulence model:

The *k-ω* turbulence model is written as:

$$\frac{D\rho k}{Dt} = \tau_{ij}\frac{\partial \bar{u}i}{\partial xj} - \beta^{*}\rho k\omega + \frac{\partial}{\partial xj}[(\mu + \sigma_{k1}\mu_t)\frac{\partial k}{\partial xj}] \quad (17)$$

$$\frac{D\rho\omega}{Dt} = \frac{\gamma 1}{vt}\tau_{ij}\frac{\partial \bar{u}i}{\partial xj} - \beta_1\rho\omega^2 + \frac{\partial}{\partial xj}[(\mu + \sigma_{\omega 1}\mu_t)\frac{\partial \omega}{\partial xj}] \quad (18)$$

The modified k-ε model is given by:

$$\frac{D\rho k}{Dt} = \tau_{ij}\frac{\partial \bar{u}i}{\partial xj} - \beta^{*}\rho k\omega + \frac{\partial}{\partial xj}[(\mu + \sigma_{k2}\mu_t)\frac{\partial k}{\partial xj}] \quad (19)$$

$$\frac{D\rho\omega}{Dt} = \frac{\gamma 2}{vt}\tau_{ij}\frac{\partial \bar{u}i}{\partial xj} - \beta_2\rho\omega^2 + \frac{\partial}{\partial xj}[(\mu + \sigma_{\omega 2}\mu_t)\frac{\partial \omega}{\partial xj}] + 2\rho\,\sigma_{\omega 2}\frac{1}{\omega}\frac{\partial k}{\partial xj}\frac{\partial \omega}{\partial t} \quad (20)$$

To obtain shear stress formulations, the k-epsilon model transport equation in equation (17 and 18) is multiplied by the blending factor F1 to get the k-ω SST model. While the equation (19 and 20) is multiplied by (1-F1) and the subsequent equations are then summarized as.

After the above transformation of the k-ε and k-ω turbulence models, the novel turbulence model after the transformation is shown by the equations written below:

$$\frac{D\rho k}{Dt} = \tau_{ij}\frac{\partial \bar{u}i}{\partial xj} - \beta^{*}\rho k\omega + \frac{\partial}{\partial xj}[(\mu + \sigma_{k2}\mu_t)\frac{\partial k}{\partial xj}] \quad (21)$$

$$\frac{D\rho\omega}{Dt} = \frac{\gamma 2}{vt}\tau_{ij}\frac{\partial \bar{u}i}{\partial xj} - \beta\rho\omega^2 + \frac{\partial}{\partial xj}[(\mu + \sigma_{\omega}\mu_t)\frac{\partial \omega}{\partial xj}] + 2\rho(1 - F1)\,\sigma_{\omega 2}\frac{1}{\omega}\frac{\partial k}{\partial xj}\frac{\partial \omega}{\partial t} \quad (22)$$

The turbulent eddy viscosity is calculated by using the following equation:

$$vt = \frac{a_1 k}{\max(a_1\omega, \Omega F2)} \quad (23)$$

Where V_t is the eddy viscosity, Ω is the absolute viscosity, a_1 is the constant, k is kinetic energy, ω is the dissipation rate, and F_1, F_2 are the blending factors [2].

2.1.2 Summary of Turbulence models

Two numerical models have been provided in ANSYS CFX solver to capture the flow turbulence, these models are k-epsilon (k–ε) and k-omega SST model (K- ω SST

model). These two models are differentiated based on application as k-epsilon (k–ε) is used for the flow away from the wall while (K- ω SST model) is used for the near boundary wall-flow or viscous sublayer. The two equations k-epsilon model is normally used to capture turbulence in engineering flow problems. However, this turbulence model cannot be used when it comes to modeling complex fluid flow problems involving high adverse pressure gradients and separation since it is not being able to predict the complex fluid flow pattern with sufficient accuracy. On the other hand, to overcome these limitations of k-epsilon and S-A turbulence models, the k-ω model is used to capture the boundary layer formation and subsequent separation. Therefore, k- ω is widely used to simulate the flow against the walls since the K-ω model has been found to predict these types of flow with reasonable accuracy. But the K- ω model has its own drawbacks and limitations. Although the k–ω model works well for the wall-bounded flows having a moderate adverse pressure gradient this model has also certain limitations, e.g. it cannot predict the pressure-induced strong separations, also the free streamflow is not accurately anticipated by this model.

In the current study k–ω Shear Stress Transport (SST) is used, which able to capture flow near the wall surface as well as in the far filed with great accuracy. SST k–ω is used where the highly accurate resolution of the boundary layer is critical, i.e. applications involving flow separation of finely resolved heat transfer profiles. The computational cost per iteration increases as the number of equations and parameters in the models' increases, so does the accuracy Fig. 4 [33][34].

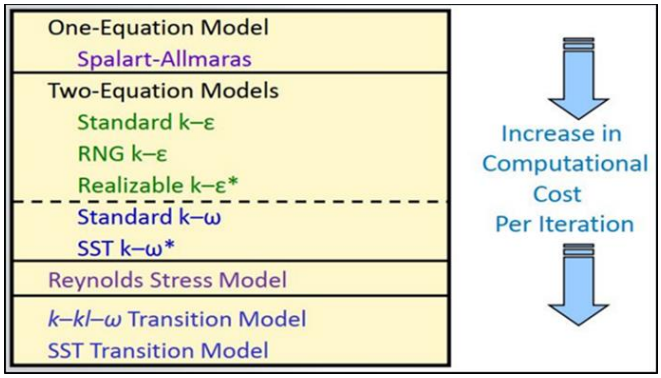

Figure 4: RANS based turbulence models

2.2 Laminar-Turbulent Transition and Separation of Flow

The most important part of the improvement of CFD is the study of the laminar-turbulent transition. The transition of the boundary layer is the transition from the laminar to turbulent flow [23]. As discussed in chapter 1, that boundary layer transition can occur on different surfaces with different mechanisms. Due to the absence of too many turbulence models that can fully capture the turbulent flows by precise simulations neither too many solvers are developed to study the laminar to turbulent flow transition.

Flow separation occurs when the flow leaves the wall due to pressure difference between the streamlines such that the streamlines velocity relative to the wall drops nearly to zero. Eddies and vortices fluid flow separate from the wall surface. Flow separation leads to enhanced drag, especially the pressure drag that occurs as it moves through the air because of the pressure-gradient between the object's front and back surfaces [35]. That is why there has been extremely great research going on, on the hydrodynamic and aerodynamic surface design that postpone the separation of flow and keep the smooth passage flow if possible. Examples include a tennis ball fur, a golf ball dimples, a glider tabulator, induce an early shift to a turbulent flow-regime; light aircraft vortex-generators to control the separation flow structure; and leading-edge extensions for the elevated angle of an incident on aircraft wings [36][37].

An eddy is the twirling of fluid in fluid dynamics when the fluid is in a turbulent flow region, the inverse current produced. The mobile fluid generates a room on the downstream side of the object free of flowing fluid. When fluid flowing enters the other side of the obstacle into the cavity or void it makes a fluid vortex on each side of the obstacle which is followed by a short inverse fluid flow other behind the obstacle flowing backstream to the back of the obstacle. To observe this naturally occurring phenomenon, the best example is the fast-flowing rivers behind large emergent rocks[38]–[40].

A vortex is a region in a fluid where the flow rotates around a line of an axis that can be curved or straight, in fluid dynamics. Vortices form in moving fluids and can be seen in smoke, rings, vortices in a boat's wake, and winds around a dust devil or

tropical tornado. Vortices are a significant element of turbulence and turbulent flows. The distribution of velocities, the idea of circulation and vorticity is used for the complete characterization of the vortices. The fluid flow speed next to its axis is the largest in most vortices and reduces in inverse proportion to the axis range[41]–[44].

Many applications like compressors, turbines, airfoils, and turbine blades the boundary layer including the transition from laminar to turbulent are the most important factors to study and understand the flow mechanism. Thus, it became the most important and essential part of computational fluid dynamics [23]. For the general coupling of computational fluid dynamics with the experimental data for the transition from laminar to the turbulent boundary layer, a turbulence-model was given by Menter et al. [32].

The turbulence model formulated by Menter et al. was γ-$Re_{\theta t}$ (Improvement in the SST turbulence model for separated flow transition prediction) consists of two components. The first part of this turbulence model combines the experimental data with the CFD codes, which is a combination of two transport equations. The second element consists of different correlations. The first component two transport equations are the equation of intermittency (γ) while the other transport equation is a transition onset momentum-thickness Reynolds number ($Re_{\theta t}$). The first component deals with the intermittency transport equation and the second equation deals with the transition from laminar to turbulent at different Reynolds number. The second part captures the transition from laminar to turbulent flow and separation on the boundary layer [45].

2.3 Influence of Roughness as a Passive Flow Control Method on Turbulent Flow Structure

The viscous sublayer of the flow composed of two layers, outer and inner layers. These two layers depend upon different parameters. The region of the inner layer where the mean velocity pattern is dependent upon the viscous sublayer scale rather than the flow length scale. In situation of flow near the wall of the channel, the viscous scale is defined as the friction Reynolds number, $Re_{\mathrm{T}} = \frac{u_T \delta}{\upsilon}$ and viscous sublayer, $\delta_\upsilon = \frac{\upsilon}{u_T}$.

While in the situation of the outer layer there is no direct effect of the viscous layer on the mean velocity pattern [46].

For the boundary layer close to the wall, turbulence theories propose a velocity shape and profile described by the viscous flow regime, where the mean velocity is given by:

$$u^+ = \frac{1}{k}\ln(y^+) + B \quad (24)$$

Where $u^+ = u/u_T$ and $y^+ = y/\delta_v$, where B is constant.

However, the local Reynolds number is considered high in the presence of roughness, in the specific condition the roughness scale is larger as compared to the viscous sublayer. High Reynolds number is specifically because of pressure forces not because of viscous stresses and in this case the momentum of the fluid that is transferred to the wall is achieved by the drag force on the roughness elements. In this case, the velocity profile is modified as [47]:

$$u^+ = \frac{1}{k}\ln\left(\frac{y}{s}\right) + B\left(\frac{s}{\delta_v}\right) \quad (25)$$

The value of B is 8.5 for the fully rough wall.

To find the difference between smooth and rough wall, the mean velocity profile shown by the equation:

$$\Delta u^+ = \frac{1}{k}\ln\left(\frac{y}{s}\right) - 3.5 \quad (26)$$

The mean velocity profile for the boundary layer is shown by the equation:

$$u^+ = \frac{1}{k}\ln\left(\frac{y}{s}\right) + B - \Delta u + \frac{2\pi}{k}\omega\frac{y}{\delta} \quad (27)$$

The above equation involves the overlap velocity region, the roughness shift Δu^+ and the π parameter, wake function. The π parameter is dependent upon the flow structure and is considered as the wake parameter. Where δ is the boundary layer thickness in the above equation [48].

The mean velocity distribution difference over both smooth and rough wall surface is shown in figure 5 given below:

The allowable roughness height is considered as the discrete element maximum roughness height which causes friction on the surface as compared to the smooth surface. The total roughness height does not affect the performance of the compressor if the wall is considered as the hydraulically smooth and the roughness height does not cross the limit of the laminar viscous sublayer. In general, the rule is "if the non-dimensional parameter, $k^+ = \frac{v^* k_s}{v} < 5$ then the wall will be specified as hydraulically smooth [49].

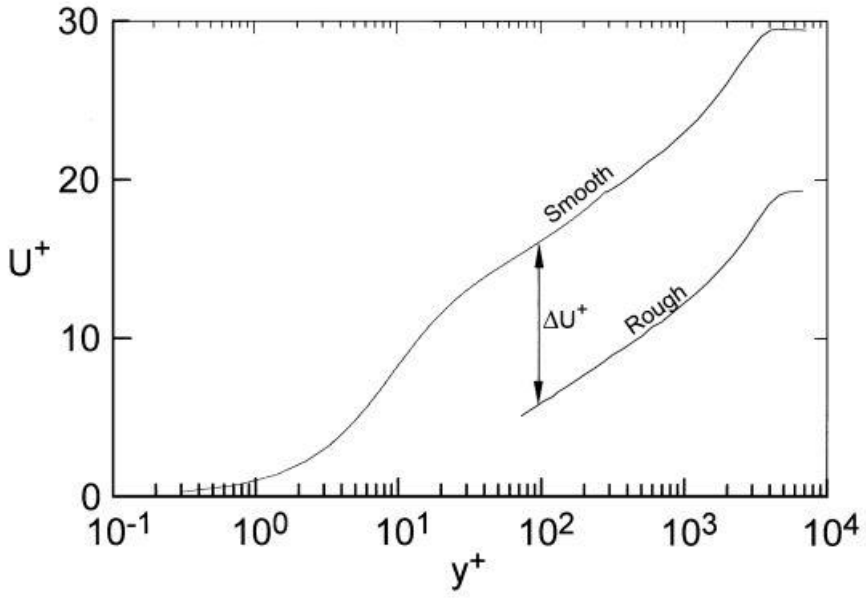

Figure 5: Mean velocity distribution for smooth and rough wall [50]

Chapter 3

Numerical Performance Evaluation of Centrifugal Compressor

This chapter describes the aerodynamics of the centrifugal compressor and the validation of experimental data using numerical simulations. The compressor used for the current analysis was developed and manufactured by the German Aerospace Center (DLR) [1]. Computational analysis has been performed to study the aerodynamics and validation of baseline centrifugal compressor and evaluate the roughness effect at steady-state simulations. To study the unsteady flow field, steady-state simulations carried out using commercial solver ANSYS CFX. The test case compressor simulations have been performed using the defined set of experimental boundary conditions and a detailed flow field has been analyzed. This chapter summarizes the flow instabilities that occur in the compressor, performance Speedline, and flow structure in the impeller passage. In this chapter, the methodology for the numerical simulations has been given and discusses the results obtained from numerical simulations.

Section 3.1 of this chapter provides the test case compressor specifications. The numerical setup and computational methodology are briefly explained in Section 3.2. Section 3.3 presents the compressor performance analysis in detail, which gives insights about the performance parameters of the compressor i.e. compressor pressure ratio and efficiency. Next, detailed compressor impeller flow field aerodynamics has been described in section 3.4. The flow instabilities evolution that occurs in the compressor due to flow separation and flow recirculation, which leads to performance degradation is discussed in section 3.5.

3.1 Compressor Specifications

A baseline centrifugal compressor having high specific speed, flow rate and pressure ratio has been simulated to study the parametric analysis of surface roughness of different magnitudes on the flow instability and performance. The baseline compressor for the current study was developed and designed by the German Aerospace Center

(Deutsches Zentrum für Luft- und Raumfahrt; DLR). The main specifications are listed in Table I.

Fig. 6 shows, test case impeller consists of a total of 26 blades with 13 full and splitter blades. At the impeller outlet domain, a vaneless diffuser is attached, and this diffuser completes the compressor stage. The compressor for the current analysis has an outer diameter of 112 mm with a splitter blade leading edge starts at 55 mm radial direction and impeller rotational speed of 50,000 rpm. The design tip clearance is variable, 0.05 cm at the blade leading edge, and 0.03 cm at the blade trailing edge.

The impeller (SRV2-O) design data are illustrated in Table I [1]:

Table I: Specifications of Baseline Centrifugal Compressor

Specifications	Data	Units
Inlet pressure, Pt1	101.3	[kPa]
Inlet temperature, Tt1	15	[°C]
Rotational speed, n	50,000	[rpm]
Mass flowrate at design point, m	2550	[g/s]
Blade flow-angle at the inlet (β_1)	26.5	-
Impeller blade tip-speed	586	[m/s]
Impeller pressure-ratio	5.8	-
Isentropic efficiency	84%	-
Full and Splitter blades count	13:13	-
Blade flow-angle at the outlet (β_2)	52	-

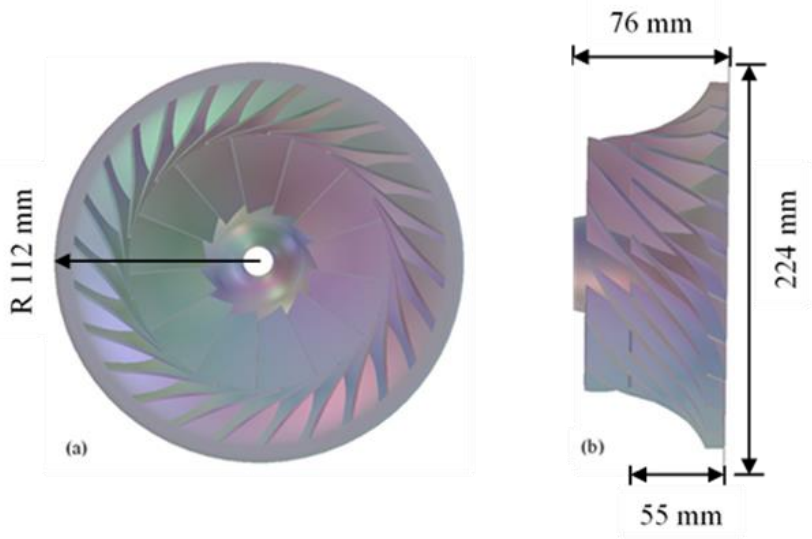

Figure 6: BladeGen Module Impeller Geometry for CFD analysis (a)Front View (b)Side View

3.2 Numerical Setup

For the CFD model to acquire, numerical simulations have been performed following step by step methodology. The stepwise numerical setup was followed in the listed steps, such as listing assumptions and the equations used, modeling of the compressor in BladeGen, creating a mesh in TurboGrid, defining the turbulence models, and feeding the boundary conditions to ANSYS CFX [51].

3.2.1 BladeGen Geometry

The initial step is modeling an accurate compressor in the BladeGen module of the ANSYS using the data provided by the German Aerospace center to acquire proper design as shown in Fig. 6 [20]. BladeGen tool is used for radial geometries, which examines 2D data and converts it into a 3D model, which provides the most accurate radial geometries for simulation purposes.

In the BladeGen module, it assembles all the components to represent it as a single domain. Using the combined data for baseline compressor Inlet, rotor, and diffuser and modeled it as a single stage of compressor is shown in Fig. 6.

3.2.2 Computational Method for Meshing

The compressor is 3D modeled in the BladeGen module of the compressor, then an H-grid mesh type has been created for the whole compressor in the TurboGrid module of ANSYS. TurboGrid is specifically used for the turbomachinery setups, this module creates refined hexahedral mesh automatically for all kind of complex turbomachinery applications. As validation is carried out using both k-ε and shear stress transport turbulence models, mesh properties have been defined accordingly. To study k-ε turbulence model, which is used for the planar shear layer away from the boundary walls, y-plus value is taken as 35 while shear stress transport model is used to study viscous sublayer near the wall, which requires refined mesh with a high number of elements, so the y-plus value of 0.001 is defined for this turbulence model. H-grid topology is used for both the turbulence models with 30 elements in each inlet and outlet. A grid independency test performed showed that the adequate number of mesh elements for the k-epsilon model and shear stress transport model are 5,60,788 and

6,02,613 respectively as there was no significant change in the pressure ratio of the compressor as shown in Fig. 7 and 8 [5],[51].

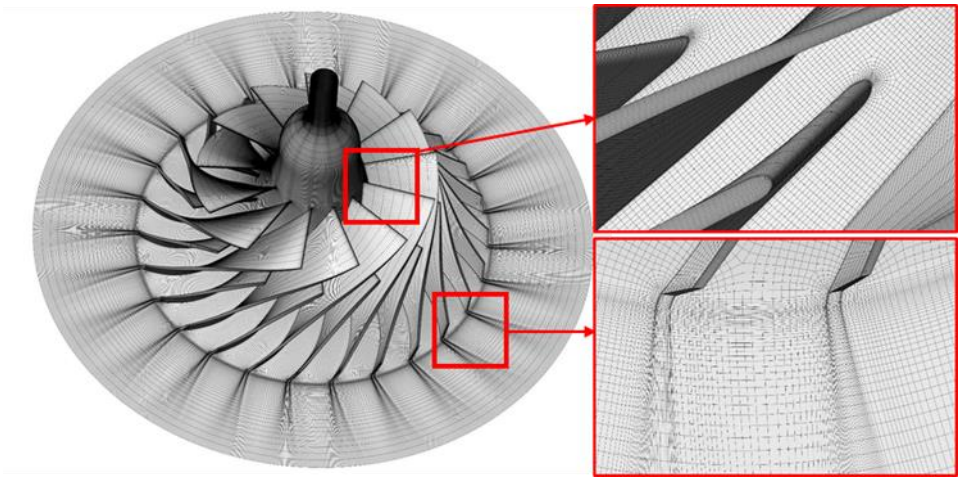

Figure 7: Computational Grid (TurboGrid Module)

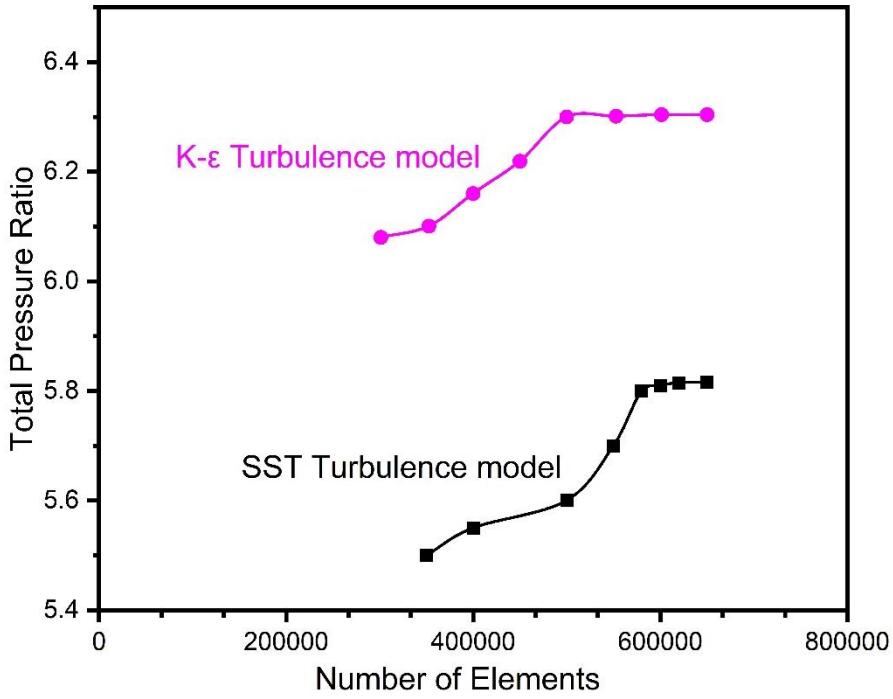

Figure 8: Mesh Independency Test

3.2.3 Turbulence Model

In the ANSYS CFX module, two turbulent flow models to capture turbulence in the flow which are k-epsilon (k–ε) and k-omega (K- ω SST) model are mostly used, turbulence models. The S-A model is a one equation model which is used for large

meshes, also it gives better results for mildly complex external and internal flows. It can be used to predict turbulence in boundary layer flows under pressure gradients such as flows over airfoils and compressor blades. It has some limitations as well, it performs very badly for 3-D flows, and free shear flows also flows with strong separation. The two equations k-epsilon model is normally used to capture turbulence in engineering flow problems. However, this turbulence model cannot be used when it comes to modeling complex fluid flow problems involving high adverse pressure gradients and separation since it is not being able to predict the complex fluid flow pattern with sufficient accuracy. On the other hand, to overcome the limitations of k-epsilon, the k- ω model is used to capture the boundary layer formation and subsequent separation. Therefore, k- ω is widely used to simulate the flow against the walls since the K-ω model has been found to predict these types of flow with reasonable accuracy. But the K- ω model has its own drawbacks and limitations. Although the k–ω model works well for the wall-bounded flows having a moderate adverse pressure gradient this model has also certain limitations, e.g. it cannot predict the pressure-induced strong separations, also the free streamflow is not accurately anticipated by this model.

In the current study both *k-ω SST* and *k-ε* models are used for the numerical investigation of test case compressor. K- ε model provides good results to study the recirculating flow streamlines away from the wall for which the Y-plus is kept 35, as the model requirement. For the SST model the value of Y+ is kept 0.001, as the criteria for the turbulence model is to keep Y-plus value equal to or less than 1. The computational cost per iteration increases as the number of equations and parameters in the models' increases, so does the accuracy Fig. 4 [29][30].

3.2.4 Boundary Conditions for Baseline Compressor

The boundary conditions specified at the inlet of the compressor are:

$$T_i = 288.15\ k \tag{28}$$

$$P_i = 101.325\ kpa \tag{29}$$

$$Convergence\ Criteria = 1 * 10^{-5} \tag{30}$$

According to standard ambient conditions, the medium turbulence intensity is kept 5% which was used by the experimental setup at DLR for a turbo setup. Mass flow rate is considered for the convergence which is recorded by slowly decreasing static pressure at outlet and the convergence criterion is taken a value of $1 * 10^{-5}$ for all residuals. As it is well known fact that pressure ratio is the smallest at choke point, so static pressure is specified in the expressions section of the CFX preprocessing, which is used to find choke point for compressor Speedline [52]. For interfaces between inlet, impeller, and diffuser, stage interfaces have been defined. The rotational periodicity has been defined across all the passages [53].

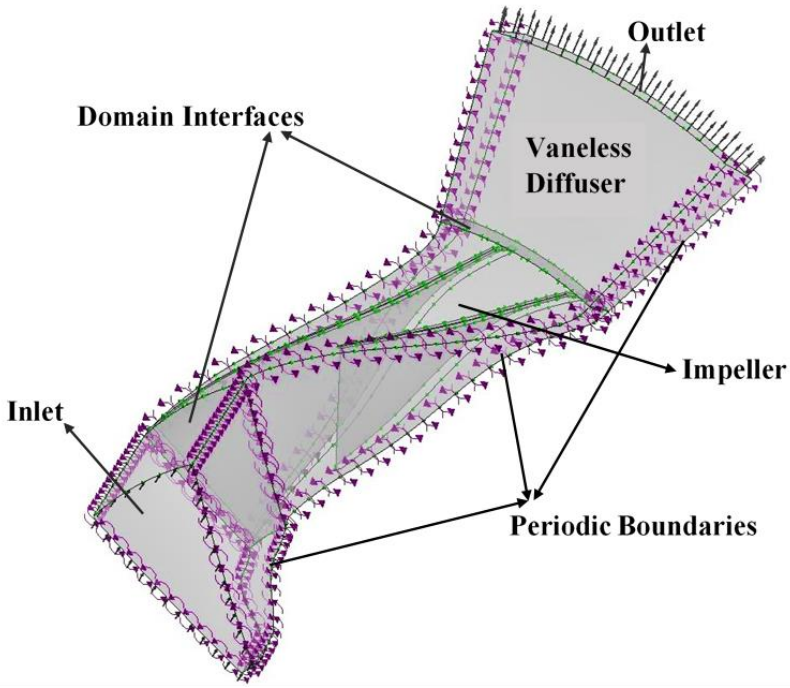

Figure 9: Computational Domain

3.3 Compressor Performance Analysis

To study the performance of the centrifugal compressor, pressure ratio, and efficiency of the compressor is calculated using numerical simulations. Theoretically, the pressure ratio can be applying the below equation [54]:

$$\boldsymbol{Pr} = \frac{\left[\int \boldsymbol{P_d} * \frac{\boldsymbol{dm}}{\boldsymbol{m}}\right]}{\boldsymbol{P_0}} \qquad (30)$$

Where P_d is diffuser outlet pressure, P_0 is impeller inlet pressure, $\dot{m}$ represents mass flow rate and P_r is the compressor pressure ratio. Efficiency can be theoretically

calculated by the below equation:

$$\eta_{tt} = \boldsymbol{T_0}(\boldsymbol{Pr}^{\frac{\gamma-1}{\gamma}} - \mathbf{1})/(\boldsymbol{T_d} - \boldsymbol{T_0}) \qquad (31)$$

Where η is the compressor isentropic efficiency, T_0 is compressor inlet temperature and T_d is compressor outlet temperature.

To numerically simulate the 3D model, several agreements are made for CFD solvers with the experimental calculations, which are listed in bullets [26]:

- K- ε and SST turbulence models are used for simulations
- Simulations conditions: mass flowrate 2.55 kg/s and rotating speed of the impeller is 50,000 rpm

Numerical simulations are performed for the Speedline from stall to choke at a constant speed of 50,000 rpm to compare with the experimental results. This comparison is carried out to show the appropriateness of this solver (ANSYS CFX) and make realistic results for further investigation and research in the compressor as shown in Fig. 10. This comparison has been made based on simulated Speedline with experimental Speedline by assessing the pressure ratio and efficiency of the compressor. The simulated and experimental Speedline is illustrated in Fig. 10. The numerical simulations overpredicted the experimental data by 8% using the k-ε model while 3% using the k-ω SST model. As it is steady-state analysis, so stall occurs either because of singular or three-dimensional separation. At a low mass flow rate, due to adverse pressure gradient flow separation occurs, consequently, the flow separates from the surface causing the recirculating flow field. Three-dimensional flow separation is because of the existence of secondary flow. Secondary, flow occurs because of the pressure gradient in the crossflow channel direction. At specific rotational speed as mass flow rate decreases near stall, blade inlet flow angle rises and hence causes to increase the incidence angle. This increase in incidence flow angle accelerates flow at the blade leading edge causing strong diffusion, which results in flow separation from the surface [2]. On the other hand, Choke occurs when the compressor operates at a maximum possible mass flow rate[55].

Fig. 10 illustrates the efficiency performance Speedline, exactly followed the experimental data trends. Choking is the phenomenon that occurs at a high mass flow rate and it occurred at the same mass flowrate as the experimental results.

It is thus determined from the present investigation that the numerical simulations are proficient of showing the performance variation and the flow and loss mechanism inside the roughened diffuser in high-pressure ratio centrifugal compressor, even though at reduced mass flow rate stall point occurred at the same mass flowrate as the experimental result but there is a certain deviation pressure ratio. This divergence is accredited to the shortcomings of the turbulence model. The working range across the Speedline for both computational and experimental result is 16%, which is found by the formula:

$$Operating\ range = (\dot{m}_{choke} - \dot{m}_{stall})/\dot{m}_{choke} \quad (32)$$

SST k–ω is used where the highly accurate resolution of the boundary layer is critical, i.e. applications involving flow separation of finely resolved heat transfer profiles. It is also found from the validation results that the SST turbulence model shows the best agreement with the overall experimental results as it overpredicts the experimental results by only 3%. Therefore, in the current study k–ω Shear Stress Transport (SST) is used for the rest of surface roughness analysis, which able to capture flow near the wall surface as well as in the far-field with great accuracy [33][34].

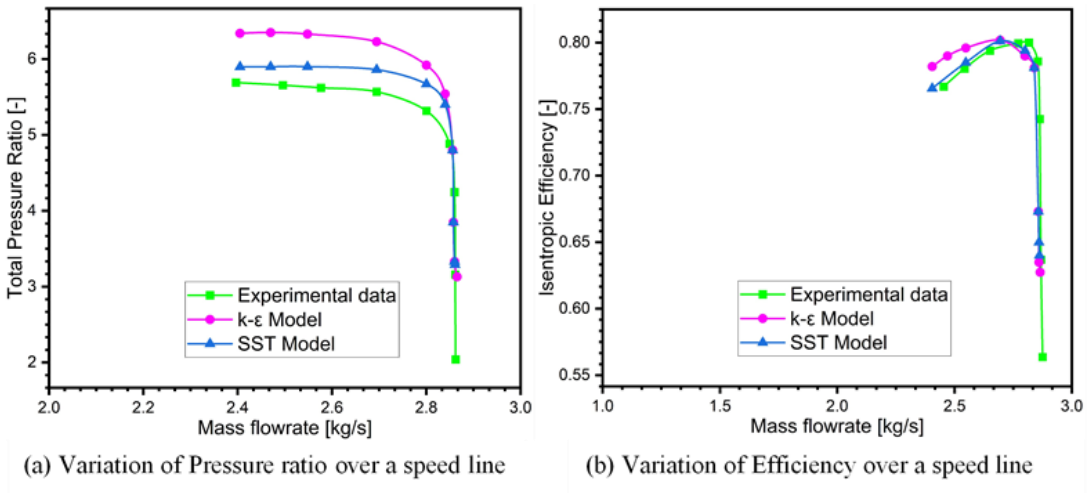

(a) Variation of Pressure ratio over a speed line

(b) Variation of Efficiency over a speed line

Figure 10: Performance map for pressure ratio and efficiency

3.4 Impeller Flow Field Analysis

Fig. 11, 12, and 13 show the contours along with the compressor impeller blades at various streamwise locations of the meridional velocity; relative Mach number; and static entropy contours.

3.4.1 Meridional Velocity

The results for meridional velocity have been analyzed at the design point. Fig. 11 shows the contours of the meridional-velocity component at various locations along the meridional length of impeller normalized on three cut planes in the exit part of the impeller at the design point. The meridional velocity represents the mass flow rate through the continuity equation, which is the absolute velocity component. The impeller shroud surface has low-velocity streamlines along the surface of both main and splitter blades.

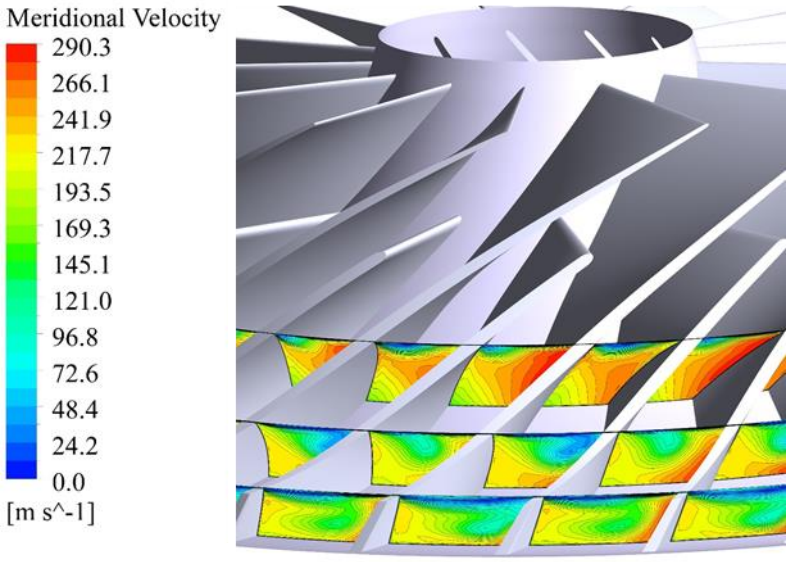

Figure 11: Meridional Velocity at Design conditions Three Cut Planes

At the hub surface and blade suction side, the largest meridional-velocity magnitudes are observed. Fig. 11 shows the inhomogeneous flow structure at the exit of the impeller having a higher blockage. Evidently, flow separation occurs at impeller shroud growing towards the impeller exit, which causes instabilities in the compressor

and higher-pressure gradients causing secondary flow losses. The separated flow stays close to the shroud surface. This wake flow expands due to reverse flow at the impeller exit close to the hub. Fig. 11 shows the meridional velocity contour along with the meridional profile. It is clear from Fig. 11 that most of the flow separation occurs at impeller exit due to which adverse pressure gradient shows flow reversal. Which results in stall phenomena in a centrifugal compressor.

3.4.2 Relative Mach Number

The contours for relative Mach number are shown in Fig. 12. A section of high Mach number is observed at leading-edge suction-side of the main blade. Along spanwise and circumferential direction a high relative Mach number increases. A relatively high mass flow rate, the Mach number is too high which results in high meridional velocity due to which blade angle is higher than the relative flow angle and positive incidence angle. In the augment of the speed of flow, the most important component is a positive incidence angle. At the inlet of the impeller, the relative Mach number is higher and then it decreases gradually and steadily. The Mach number region decreases both in the spanwise and streamwise direction and lowest at the exit of the impeller shroud. The reason behind the decrease in relative Mach number and flow velocities is attributed to tip-leakage flows.

3.4.3 Static Entropy

Fig. 13 represents static entropy generation contours in the passage between the main and splitter blade. Most of the losses appear to occur in the impeller exit domain because of wake development and secondary flow. It is evident from Fig. 13 that most of the losses appear to occur at the shroud surface of the impeller. The largest loss region appears to occur at the trailing edge shroud. This loss region is mainly because of large tip-clearance flows which immensely influence the core flow.

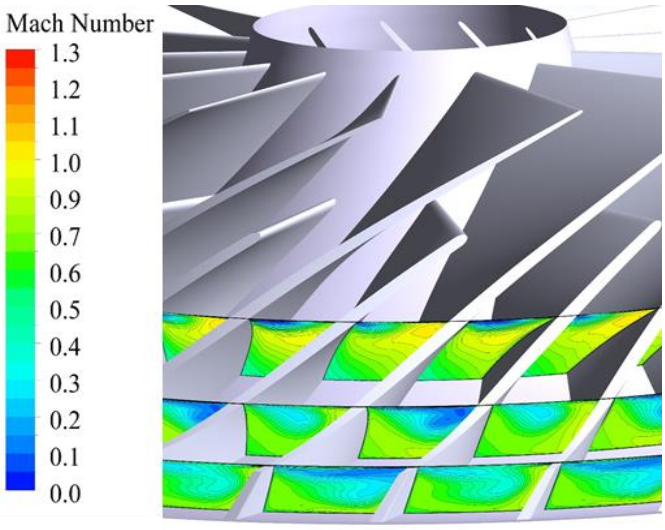

Figure 12: At Streamwise locations, Mach Number along with the impeller

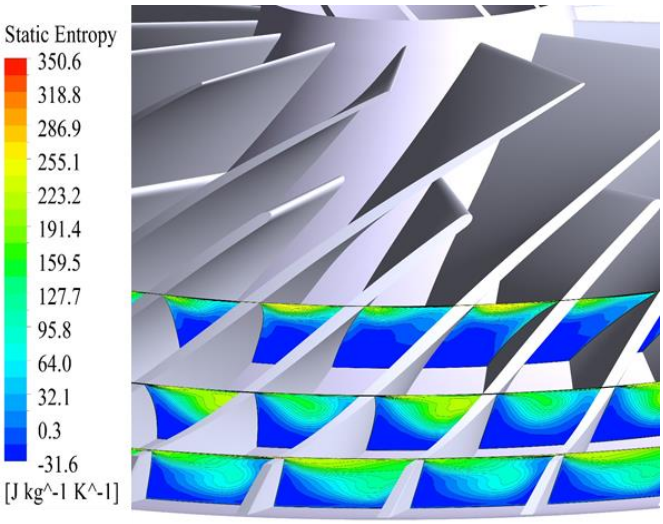

Figure 13: Static Entropy Generation at Design Condition

3.4.4 Static pressure Rise

Fig. 14 show the static pressure rise measured along the impeller stage for three points at design speed; stall point, design point and choke point. A very steady static pressure rise occurs at the design mass flow rate ($\dot{m}_{design}$ = 2.54 kg/s), which is the highest static pressure rise across the compressor stage. A chokepoint the static pressure rise

is very small due to high Mach-number at the outlet of the impeller. The dislocation effects at the main blade and splitter blades leading edges are openly imitated by static pressure rise, which is decreasing with increasing mass flow rate as illustrated in Fig. 14. The least static pressure occurs at the choke point. A chokepoint, due to high relative Mach number static pressure drop occurs in the impeller region and as the flow enters the diffuser section static pressure rise starts there. The inducer flow is stalled at 16% of flow margin, calculated by equation 4 [7]:

$$\text{Flow margin}=1-\left(\frac{\dot{m}_{stall}}{\dot{m}_{choke}}\right)$$

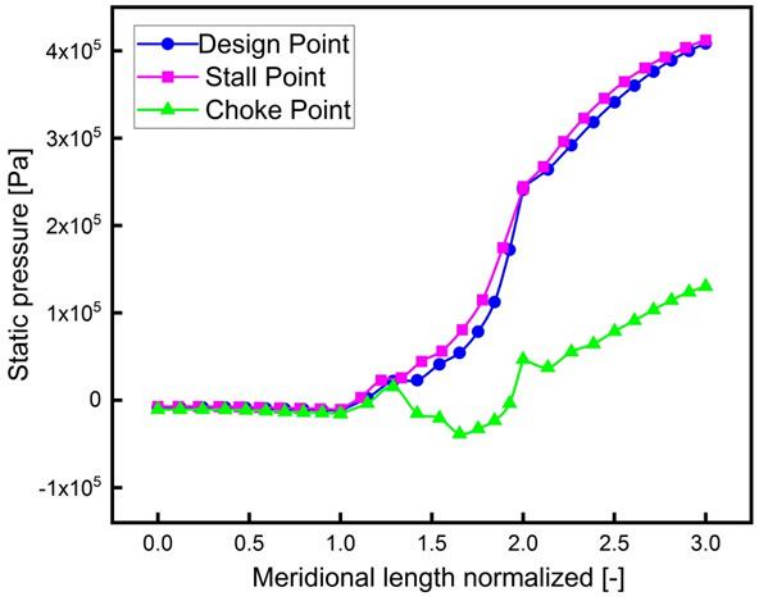

Figure 14: Static Pressure Rise at Different Operating Points

3.5 Evolution of Flow instabilities

The performance evaluation of the test case compressor at various working points from choke to stall point along the Speedline has been evaluated in section 3.3. As most of the flow instabilities happen at a low mass flow rate, so most of this section describes the flow behavior because of a decrease in mass flow rate. When compressor at low mass flow rate is simulated, all the factors and phenomenon that caused compressor flow instabilities has been observed. All those factors that lead to flow instabilities are the flow separation, flow recirculation, and flow reversal due to adverse pressure gradient and this phenomenon leads to surge and stall of the compressor and it has

been observed at a low mass flow rate. Numerical simulations at low mass flow rate showed all signs and peculiarities responsible for the development of these unstable flow regimes. These flow instabilities are flow separation from the surface, wake/jet flow, recirculation flow, and other such instabilities which cause the compressor to stall [22].

The working of the compressor at a low mass flow rate causes the flow to separate at the impeller exit near the shroud surface, which results in the development of jet/wake regions of adverse pressure gradients. The reason behind the flow separation is adverse pressure gradient and secondary flow. The flow pattern contours at impeller midspan are shown for all the three important operating points, stall, design, and choke point.

3.5.1 Inlet Recirculation Region

It is a stationary phenomenon that occurs in the inlet region of the centrifugal compressor. This flow instability occurs at the inlet of the compressor and increases pressure in radial machines at the outlet of the impeller. It gives the very first sign of flow instability in the compressor. To show the inlet recirculation regimes in the compressor meridional velocity contours and velocity vectors along the meridional plane are shown in Fig. 15 [5].

The operating range of the compressor is greatly affected by the flow recirculation. Though, this kind of flow instability may lead to a deep surge in high-pressure ratio compressors [56]. As depicted in Fig. 15 that this phenomenon can be seen at an extremely high flow rate which develops recirculation regions on the shroud of the impeller. These recirculation regions can be seen at high peaks when the mass flow rate decreases from the design point and converge towards the stall point as illustrated in Fig. 15a.

3.5.2 Flow Separation Within Impeller

The flow separation within the impeller affects the stable operating range of the centrifugal compressor. The non-uniform flow phenomena occur as a result of complex three-dimensional flow but the instabilities in the complex flow field occur as a consequence of flow separation and flow reversal.

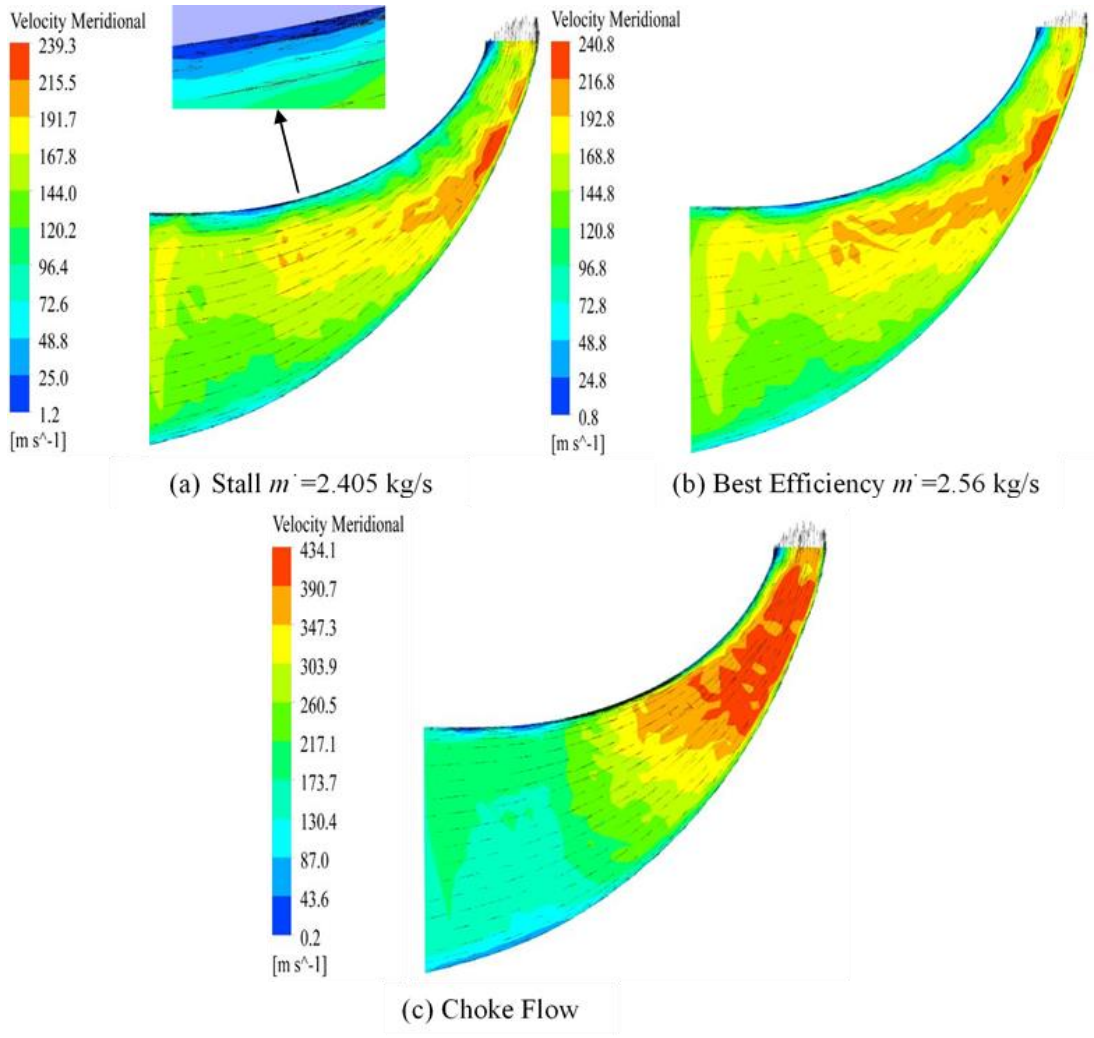

Figure 15: Meridional Velocity Contour at the impeller midplane for different flow rates

. Flow instabilities as a result of flow separation and flow recirculation and its effect on the performance of the compressor can be seen from Fig. 16. At high incidence angle and low mass flow rate, flow separates from the leading edge of the blade and the main and splitter blade suction side. When flow enters at the impeller eye axially and then move towards radial direction due to Coriolis forces. Depending upon the velocities of the streamlines, these forces act on different streamlines differently. During this phenomenon, high-velocity streams try to move away from the low-velocity streams, and thus this phenomenon forms the secondary flow and it leads to flow separation in the compressor due to adverse pressure gradient.

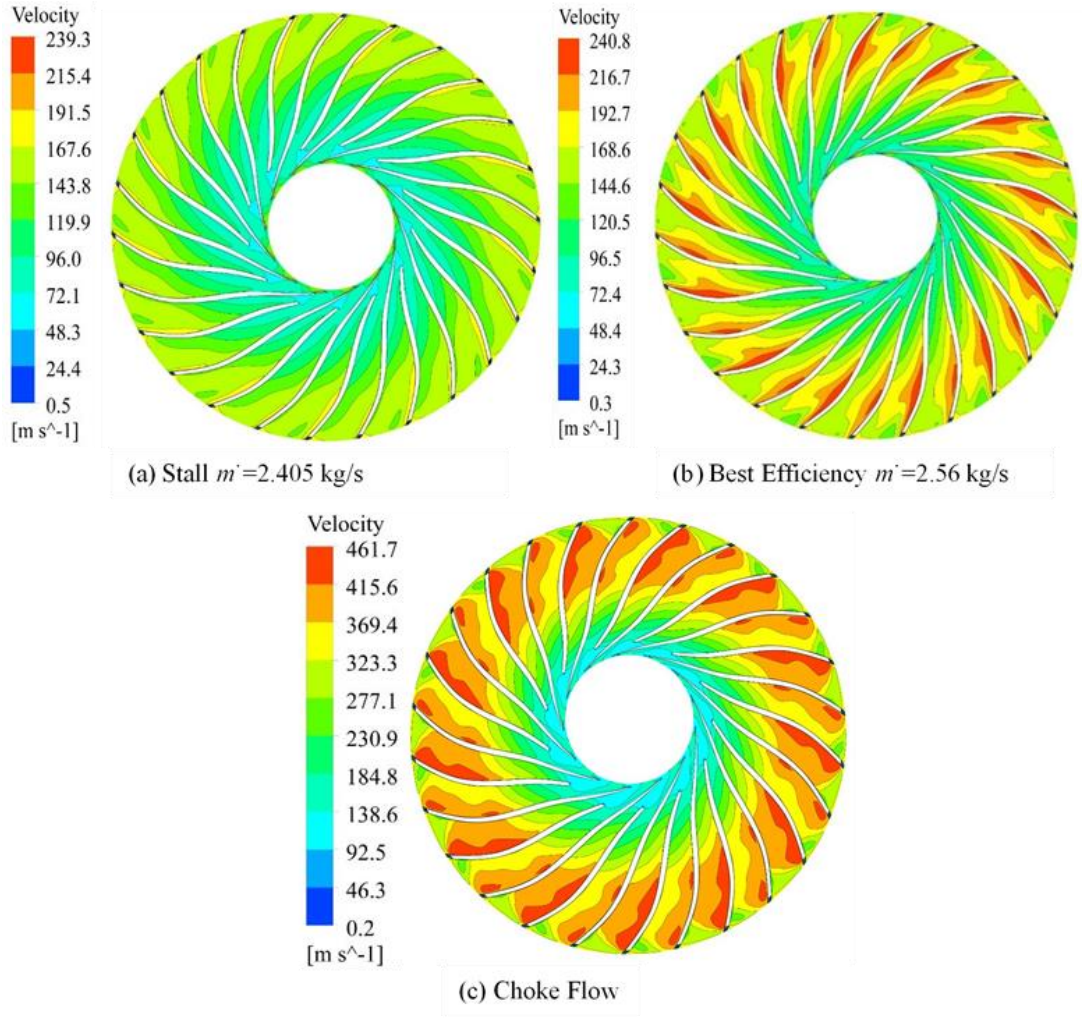

Figure 16: Relative velocity contours of the impeller domain

When flow separates from the walls or boundary layers of the compressor, it starts to create low energy wakes and vortices. Secondary flow streamlines at low mass flow rate affecting the core flow have been depicted in Fig. 17. The indication of these streamlines depicts the development of flow instabilities in the compressor.

3.5.3 Diffuser Shroud Flow Separation

As it is a well-known fact that flow separation causes instability in turbomachines performance and should be avoided. In the same way, the phenomena has a great impact on the centrifugal compressor performance as well. Stall phenomena under steady-state conditions occur in the diffuser section of the compressor because of flow separation due to adverse pressure gradient. This local flow separation at the diffuser

shroud occurs at a small mass flow rate because of skewed flow, which leads to a rotating stall.

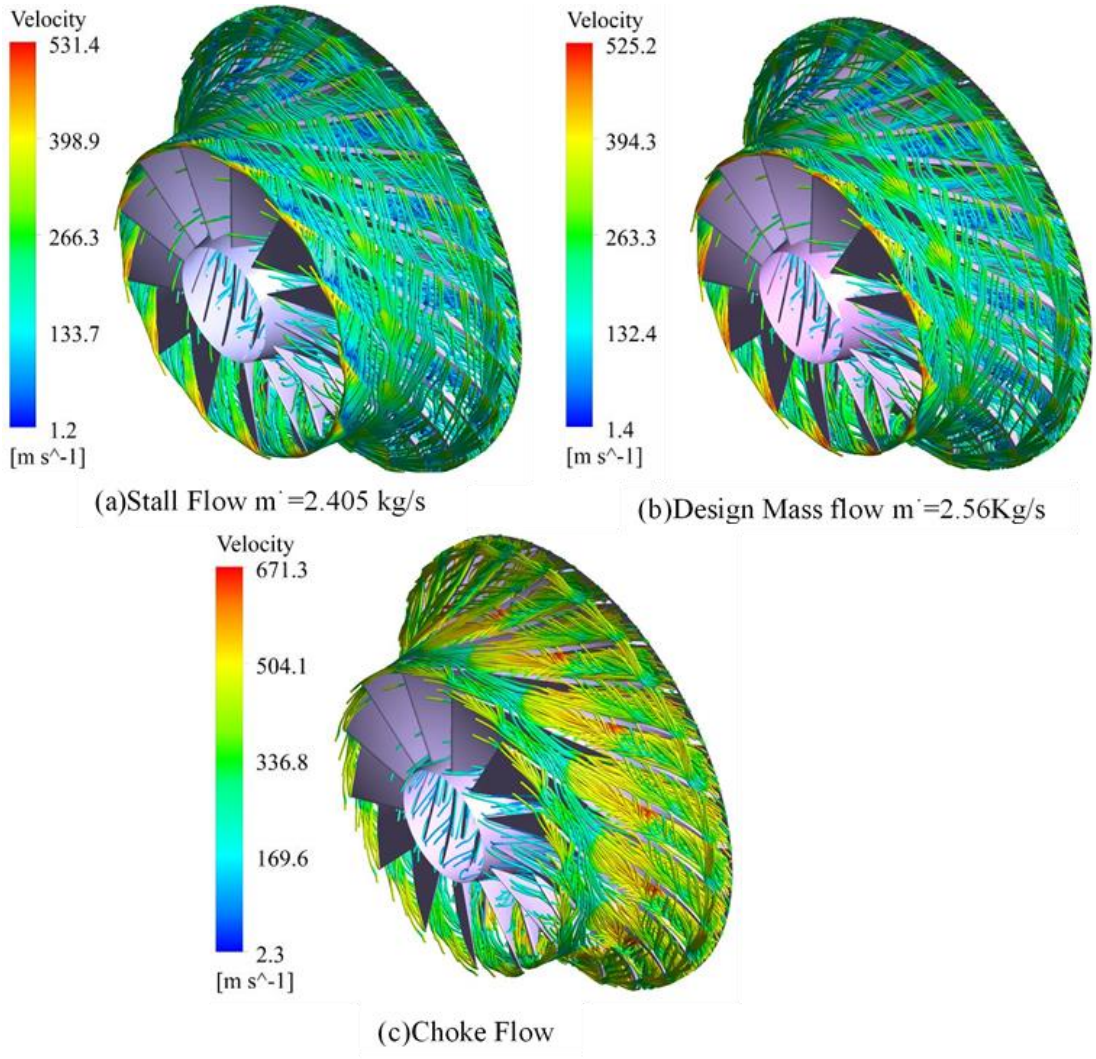

Figure 17: Secondary flow structure using Relative velocity streamlines

To reduce flow reversal and flow recirculation and augment the operating range of the compressor, there are many techniques called passive flow control methods are applied. These methods include surface roughness, vortex generators on diffuser shroud, and the cavity can help reduce this flow separation by compensating on pressure ratio and efficiency [2]. Fig. 18 illustrates the flow separation from the diffuser shroud as a result of the drop in the mass flow rate. As the mass flow rate approaches the stall point, flow separation reaches the maximum peak, and hence it is concluded maximum flow instability occurs at a low mass flow rate.

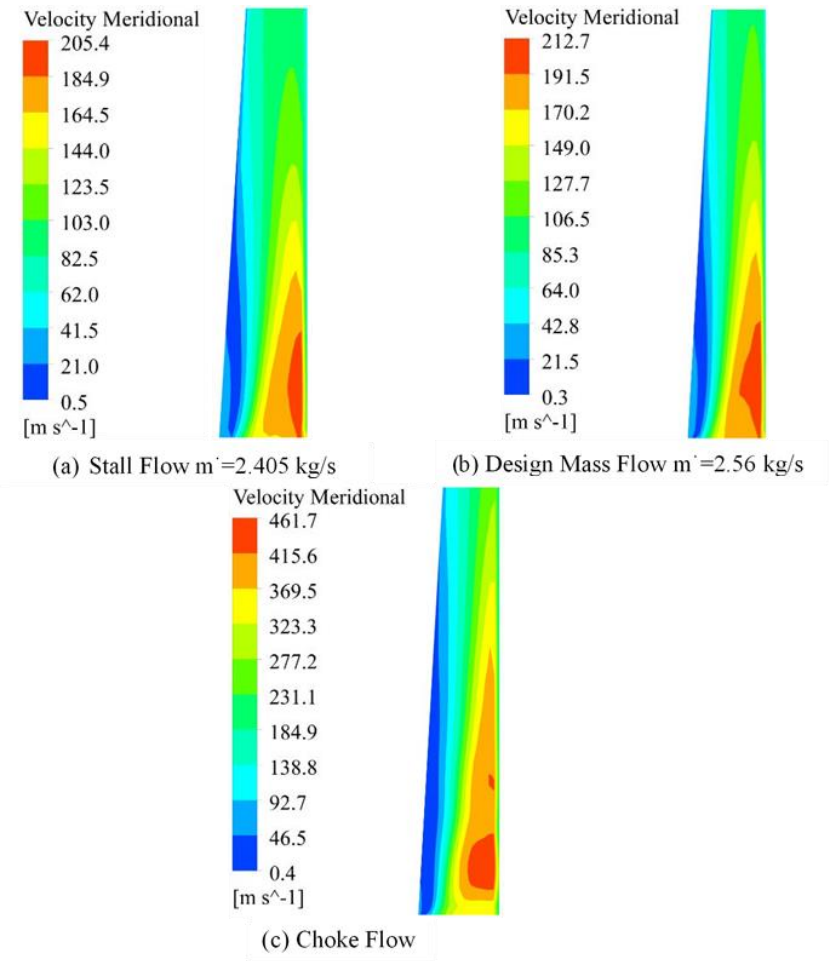

Figure 18: Flow separation at Diffuser shroud

Chapter 4

Results and Discussions

The previous chapter highlights the numerical aerodynamics of test case high-pressure ratio centrifugal compressor to foresee its performance using numerical simulations. Flow instabilities that develop due to a decrease in mass flow rate within the compressor have also been discussed in addition to aerodynamics. In this chapter the influence of the application of surface roughness parametrically on the diffuser shroud using both k-ε and SST turbulence model has been presented. The surface roughness is applied on the diffuser shroud and performance Speedline have been drawn for each roughness height to optimize the most effective surface roughness. Numerical simulations have been performed at a mass flow rate from choke to stall as shown in the performance Speedline, to study the effect of surface roughness on the flow behavior. Firstly, the effect of surface roughness on the performance of the compressor and its effect on flow stabilization has been carried out using the k-ε model and then the same analysis is performed using the Shear stress transport model. The roughness is engineered on the diffuser shroud to control flow separation from diffuser shroud and its influence on the flow structure has been examined.

4.1 Wall Surface Roughness Analysis

This section of the chapter deals with wall surface roughness by increasing the wall surface roughness from smooth surface to 200μm on impeller and diffuser surface and analyze the consequence of surface roughness on the performance of centrifugal compressor by illustrating the performance maps for each roughness height. The diffuser shroud of the compressor for the application of surface roughness has been chosen based on flow separation and flow reversal explained in chapter 3. As shown in Fig. 7 to Fig. 16 in chapter 3, a significant amount of flow reversal and flow separation occur at low mass flow rate/stall flow. Also, the flow field separates at the trailing edge of the blade as shown in Fig. 3-16. Lastly, the application of surface roughness on the impeller shroud is to reduce the flow recirculation in the impeller to the extent, that further, it does not affect the performance of the compressor.

Table II shows the roughness heights specified to be applied to the diffuser shroud. Based on the previous literature, the smooth metal surface has normally roughness of about 3.18mm and in the analysis carried out in chapter 3 shows that still there is flow reversal and recirculation [20]. So, in order to reduce flow reversal and flow recirculation, the roughness of height 50 to 200μm has been applied. The magnitude of applied roughness has been mentioned in the table:

Table II: Magnitude of roughness heights

S. No.	Roughness Height (mm)
1	50
2	100
3	150
4	200

The influence of the application of surface roughness heights on the flow structure has been investigated discretely for k-ε and SST turbulence model on diffuser shroud for each roughness height. The following section provides details about the roughness results and analysis of the flow. Then, in the next portion the roughness on the diffuser shroud has been studied and the effect on the stalled diffuser has been explained. Lastly, a brief description is added about flow reversal and flow separation.

4.2 Influence of Roughness Heights on the diffuser flow structure Using K-Epsilon Model

Fig. 19 illustrates the contours across the diffuser meridional plane for several roughness heights on the diffuser shroud. The effect of different heights of roughness on flow reversal and flow separation on the diffuser shroud is depicted in Fig. 19. This figure also illustrates the comparison of smooth surface with engineered rough surface case. As the analysis is carried out for all the cases of surface roughness, flow reversal and flow separation have been found in each case near the shroud surface of the diffuser. The presence of this flow at the inlet of the diffuser can be because of the unsteady and the viscous flow. At the impeller exit strong fluctuations in the flow

angles and the meridional velocity form extremely complicated flow patterns at impeller outlet. It is also observed that the jet/wake region exists at the exit of the impeller. At the blade pressure side, jet flow structure exists which results in the flow-reversal accumulated near the shroud surface of the diffuser. The jet flow region on the blade pressure side is considered as loss-free but it creates a low-velocity region at impeller outlet or diffuser inlet, which transports turbulence, losses and accumulates near the shroud of the diffuser. This gives a better explanation of the flow-reversal and flow-separation on the diffuser shroud surface.

Fig. 19 illustrate that shroud surface of the compressor when studied for the smooth wall, a recirculated flow was found along the diffuser shroud wall. The application of engineered roughness heights has a substantial influence on the performance and flow structure of the compressor. As roughness height has been augmented from a smooth surface to 200μm, the substantial effect has been observed in the form of a decrease in the flow reversal and flow separation at the impeller outlet. From the current examination, a significant decrease in flow separation is observed in the roughness case of 100μm and 200μm. The augment in surface roughness on the diffuser shroud causes the reattachment of flow and therefore reduces flow reversal on the diffuser shroud surface. Figs. 19(b), 19(c), and 19(d) show the consequence of the increasing roughness heights on the diffuser shroud to reduce the flow-reversal of the compressor flow field. The increase in the surface roughness eliminates the flow reversal and flow separation of the reversed flow region of diffuser shroud.

It is evident from Fig. 20, that application of surface roughness has a great impact on the performance. A steady-state simulation is executed at a stall mass flow rate of 2.366 kg/s and a rotational speed of 50,000 rpm to evaluate the performance for the centrifugal compressor at smooth diffuser shroud and at different roughness magnitudes (50μm, 100μm, 200μm). There is a pressure ratio drop with the applications of surface roughness magnitudes on the diffuser shroud.

The drop in pressure ratio has started when the roughness magnitude has been incrementally increased from 50 μm to 200 μm as shown in Fig. 20. This loss in pressure ratio is attributed to the frictional losses and thick boundary layer in the

diffuser section, which leads to an increase in surface blockage. The percentage drop in pressure ratio at the stall point for 50 μm is 3.1 %, 3.3 % for 100 μm and 3.5 % for 200 μm using the k-ε model, which offers very good results when the analysis is carried out away from the wall of the compressor but it does not give realistic results for the viscous sublayer and to study viscous sublayer, SST Turbulence model is discussed in the next section.

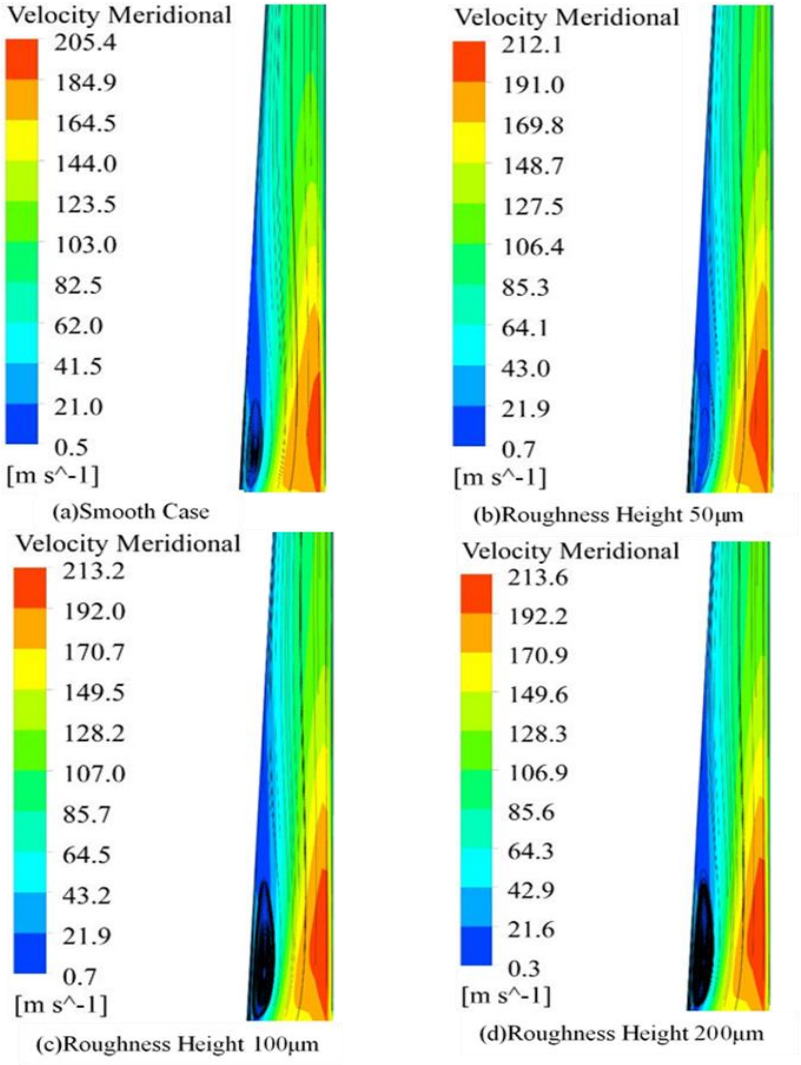

Figure 19: Diffuser Meridional plane, Meridional velocity streamlines for different roughness heights for the k-ε model

Fig. 21 shows the streamwise location of the diffuser section, which is used to calculate radial and tangential velocity from hub to shroud at each location along the meridional plane for smooth and roughened surfaces. These locations significantly define the

behavior of flow at each streamwise location. These streamwise locations are based on flow recirculation and flow reversal positions along with the diffuser shroud to hub normalized from 0 to 1.

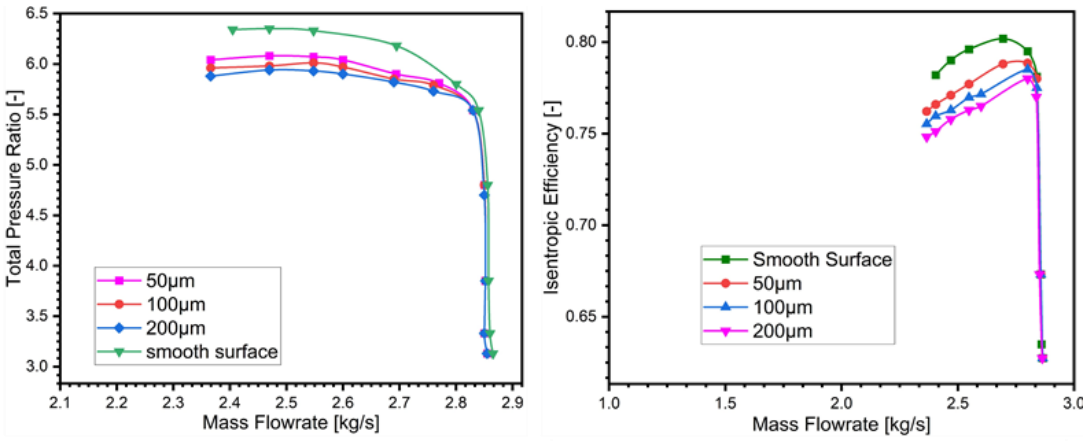

(a) Variation of Pressure ratio over a speed line for different Surface Roughness

(b) Variation of Efficiency over a speed line for different Surface Roughness

Figure 20: Performance Map for each surface roughness magnitude

Figure 21: Streamwise locations for Radial and Tangential Velocity

Fig. 22 depicts the influence of different roughness magnitudes on radial spanwise distribution at the meridional plane of the diffuser. The location and spanwise distribution of radial velocity are based on the end wall from hub to shroud of the diffuser and has been normalized from 0 to 1. As shown in Fig. 22, that reverse flow zones for all the simulated cases occur at the inlet of the diffuser. However, an

augmentation in the roughness magnitude reduces the flow recirculation. Therefore, augment in the roughness magnitude can reduce the flow separation and flow reversal. It also stabilizes the flow at diffuser shroud.

At streamwise location 1, it is evident from Fig. 22 that at diffuser inlet the roughness magnitude from 50µm to 200µm eliminates the flow reversal. Exactly, similar results are observed for downstream locations as well. The best performance stability wise is shown by surface roughness magnitude of 200µm in comparison with the smooth case. As compared to the smooth case, roughness magnitude from 100µm to 200µm completely eliminate the flow separation and exhibit a complete elimination of flow instability.

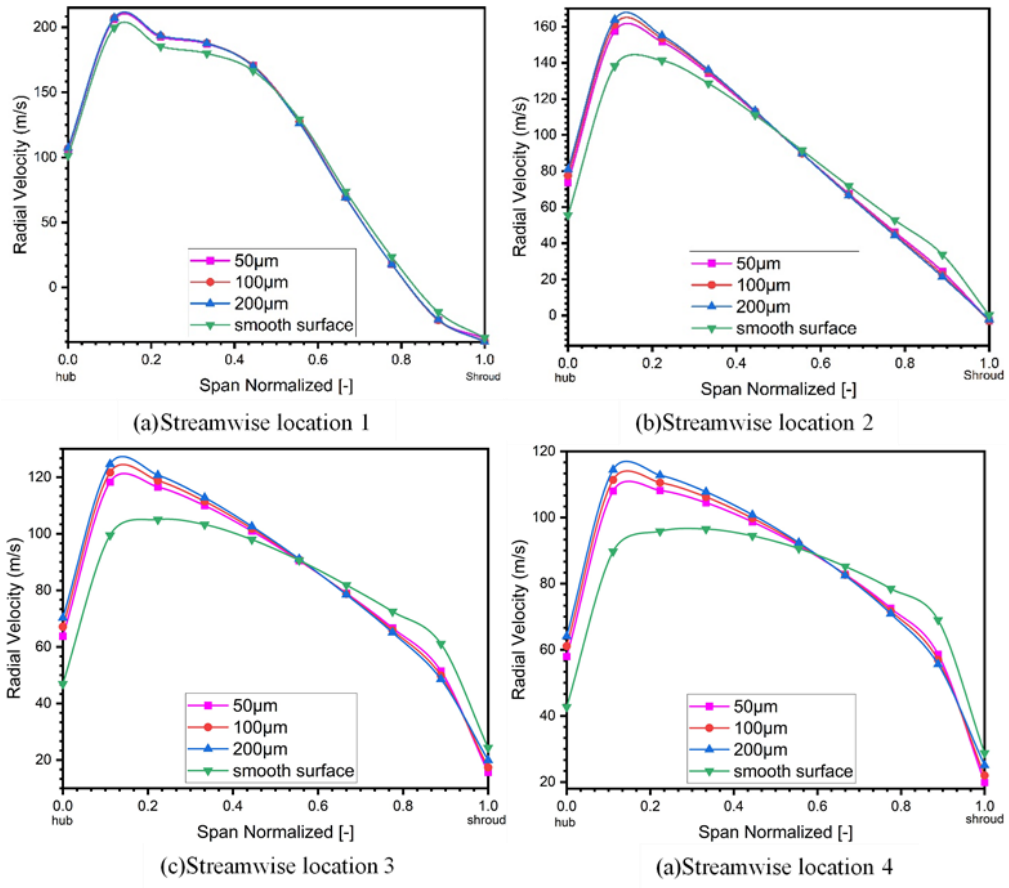

Figure 22: Radial velocity in the diffuser section at 4 streamwise locations

Even though, the case of 50µm also reduces the flow separation but still there exists a section of small flow separation at the end of the diffuser exit. Furthermore, the

ultimate radial velocity also moves in the direction of the hub of the diffuser. This transfer in the radial velocity summit is because of the growth in the thickness of the boundary layer at the shroud surface as a result of the application of roughness on the diffuser shroud.

It is seen from Fig. 22(d) and 23(d) that the flow separation at the outlet of the diffuser exists in the case of the smooth surface while the flow separation has been eliminated in the case of the roughened surface of different magnitudes. The most stable roughness magnitude is 200μm, but it significantly affects the performance of the compressor by reducing pressure ratio and efficiency as shown in Fig. 20.

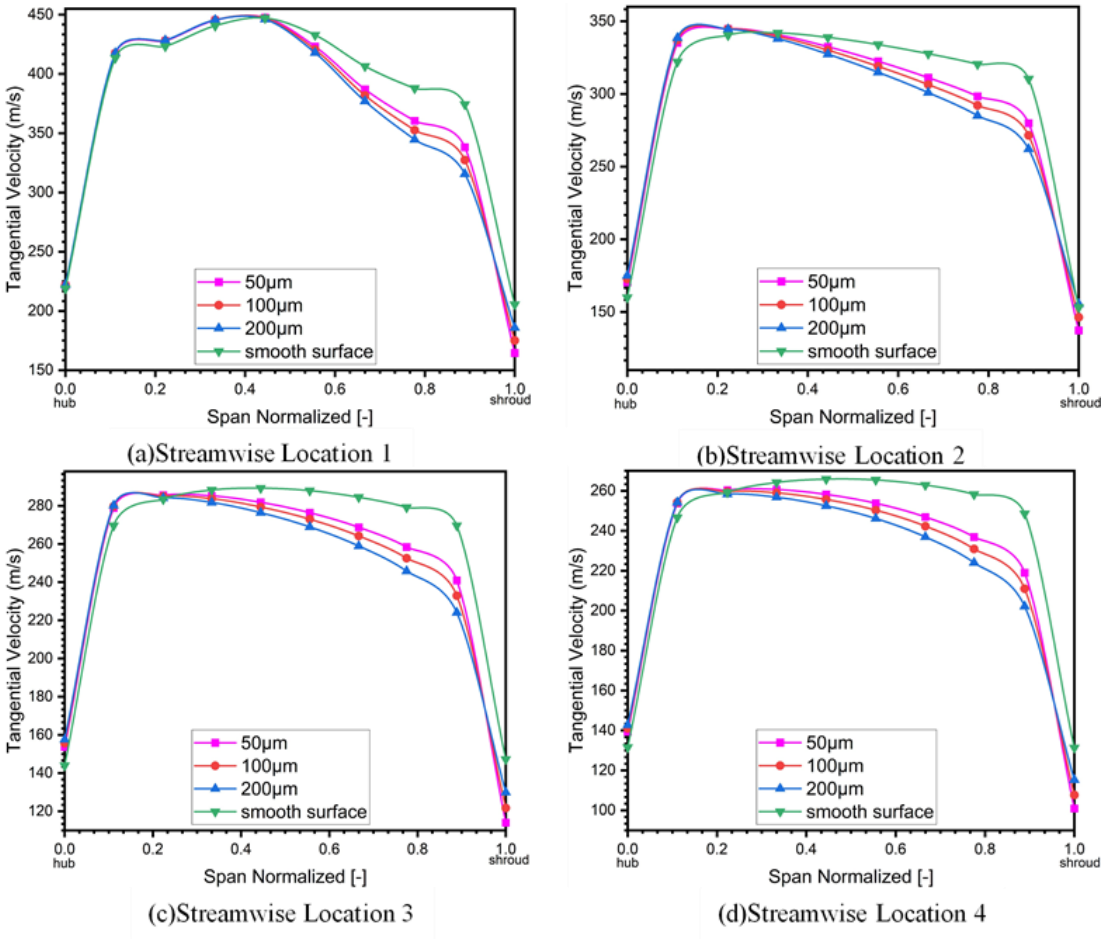

Figure 23: Tangential velocity in the diffuser section at 4 streamwise locations

It is shown in Fig. 23 at different streamwise locations along the diffuser's meridional plane tangential velocity has been distributed spanwise at four different locations. It is evident from Fig. 23 that an increase in surface roughness greatly affects the tangential

velocity of the compressor. It is noted that on each streamwise location there is a great reduction in the tangential velocity of the compressor, which results in the overall performance reduction of the turbomachine (i.e. Centrifugal compressor). This diminution in high tangential velocity is due to a reduction in the frictional losses, which counterweighs for the performance deterioration [2].

4.3 Influence of Surface Roughness heights on the Diffuser Flow Structure Using SST Model

K-ε model gives a better result for the planar shear layer and the SST Turbulence model gives realistic results to study viscous sublayer. In the current study k–ω Shear Stress Transport (SST) is used, which able to capture flow near the wall surface as well as in the far filed with great accuracy. SST k–ω is used where highly accurate resolution f boundary layer is critical, i.e. applications involving flow separation of finely resolved heat transfer profiles. The computational cost per iteration increases as the number of equations and parameters in the models' increases, so does the accuracy [33][34]. Fig. 25 illustrates the contours on the meridional plane of the diffuser shroud for various roughness heights. The effect of different heights of roughness on flow reversal and flow separation on the diffuser shroud is depicted in Fig. 25. This figure also illustrates the comparison of smooth surface with engineered rough surface case. As the analysis is carried out for all the cases of surface roughness, flow reversal and flow separation have been found in each case near the shroud surface of the diffuser. This flow field at diffuser inlet can be because of the unsteady and the viscous flow. At the impeller exit, strong fluctuations in the flow angles and the meridional velocity creates extremely complicated flow pattern at impeller outlet. It is also observed that the jet/wake region exists at the exit of the impeller. At the blade pressure side, jet flow structure exists which results in the flow-reversal accumulated near the shroud surface of the diffuser. The jet flow region on the blade pressure side is considered as loss-free but it creates a low-velocity region at impeller outlet or diffuser inlet, which transports turbulence, losses and accumulates near the shroud of the diffuser. This gives a better explanation of the flow-reversal and flow-separation on the diffuser shroud surface.

Fig. 25 illustrate the shroud surface of the compressor when studied the smooth wall, a backflow section was found on the shroud of the diffuser. The application of engineered roughness heights has a substantial influence on the performance and flow structure of the compressor. As roughness height has been augmented from a smooth surface to 200μm, the substantial effect has been observed in the form of a decrease in the flow reversal and flow separation at the impeller outlet. From the current study, it is observed that a significant decline in separation from the wall in the roughness case of 100μm and 200μm. The augment in surface roughness on the diffuser shroud causes the reattachment of flow and therefore reduces flow reversal on the diffuser shroud surface. Figs. 25(b), 25(c), and 25(d) show the consequence of the increasing roughness heights on the diffuser shroud to reduce the flow-reversal of the compressor flow field. The increase in the surface roughness eliminates the flow reversal and flow separation of the reversed flow region of diffuser shroud.

It is evident from Fig. 24, that application of surface roughness has a great impact on the compressor performance. A steady-state simulation has been executed at a stall mass flow rate of 2.366 kg/s and a rotational speed of 50,000 rpm to evaluate the performance for the centrifugal compressor at a smooth diffuser shroud and at different roughness magnitudes (50μm, 100μm, 200μm) using SST turbulence model. There is a pressure ratio drop with the applications of surface roughness magnitudes on the diffuser shroud.

The drop in pressure ratio has started when the roughness magnitude has been incrementally increased from 50 μm to 200 μm as shown in Fig. 24. This loss in pressure ratio is attributed to the frictional losses and thick boundary layer in the diffuser section, which leads to an increase in surface blockage. The percentage drop in pressure ratio at stall point for 50 μm is 3.3 %, 4.2 % for 100 μm and 5.08 % for 200 μm using the k-ω SST turbulence model.

Fig. 26 depicts the influence of different roughness magnitudes on radial spanwise distribution at the meridional plane of the diffuser. The location and spanwise distribution of radial velocity are based on the end wall from hub to shroud of the diffuser and has been normalized from 0 to 1.

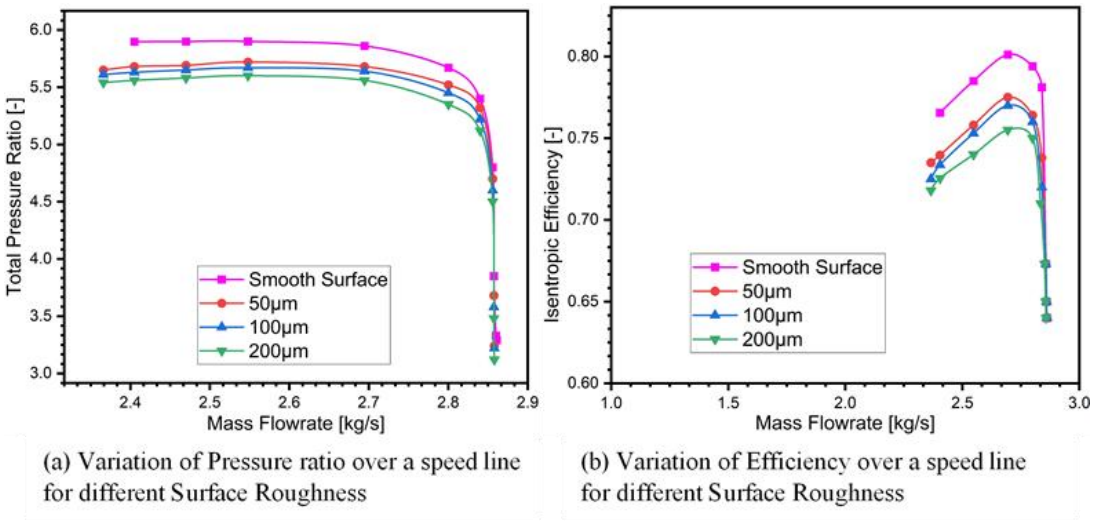

(a) Variation of Pressure ratio over a speed line for different Surface Roughness

(b) Variation of Efficiency over a speed line for different Surface Roughness

Figure 24: Performance maps for different roughness magnitudes

As shown in Fig. 22, that reverse flow zones for all the simulated cases occur at the inlet of the diffuser. However, an augmentation in the roughness magnitude reduces the flow reversals. Hence, rise in the magnitude of roughness can reduce the flow separation and flow reversal. It also stabilizes the flow at diffuser shroud.

At streamwise location 1, it is evident from Fig. 25 that at diffuser inlet the roughness magnitude from 50μm to 200μm completely eliminates the flow reversal. It also shows that the k-ω SST turbulence model shows flow reversal and flow separation more accurately than the k-ε turbulence model. Exactly, similar results are observed for downstream locations as well. The best performance stability wise is shown by surface roughness magnitude of 200μm as compared to smooth surface. As compared to the smooth case, magnitude of roughness from 100μm to 200μm completely eliminate the flow separation and exhibit a complete elimination of flow instability.

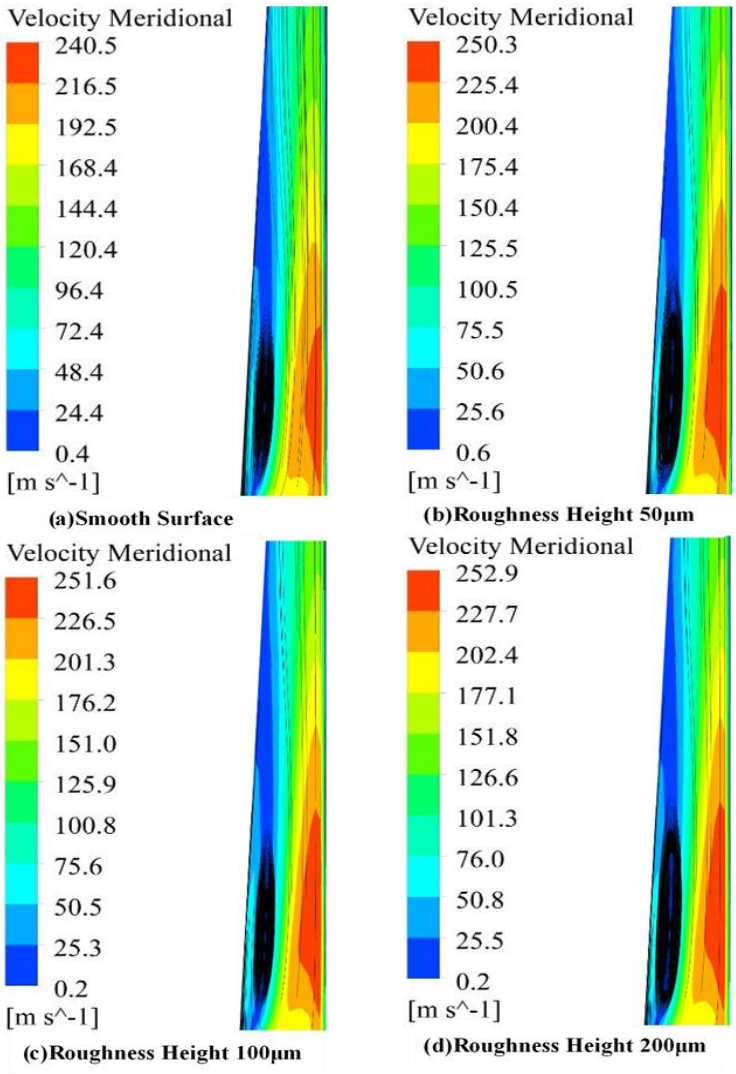

Figure 25: Diffuser Meridional plane, Meridional velocity streamlines for different roughness heights for the SST model

Even though, the case of 50µm also reduces the flow separation but still there exists a section of small flow separation at the end of the diffuser exit. Furthermore, the maximum radial velocity also moves towards the diffuser hub. This transfer in the ultimate radial velocity is because of thick boundary layer at the shroud surface due to application of roughness on the diffuser shroud.

It is seen from Fig. 25(d) and 26(d) that the flow separation at the outlet of the diffuser exists in the case of the smooth surface while at 200 µm roughness height the flow separation is negligible. The most stable roughness magnitude is 200µm, but it

significantly affects the performance by reducing pressure ratio and efficiency as shown in Fig. 24.

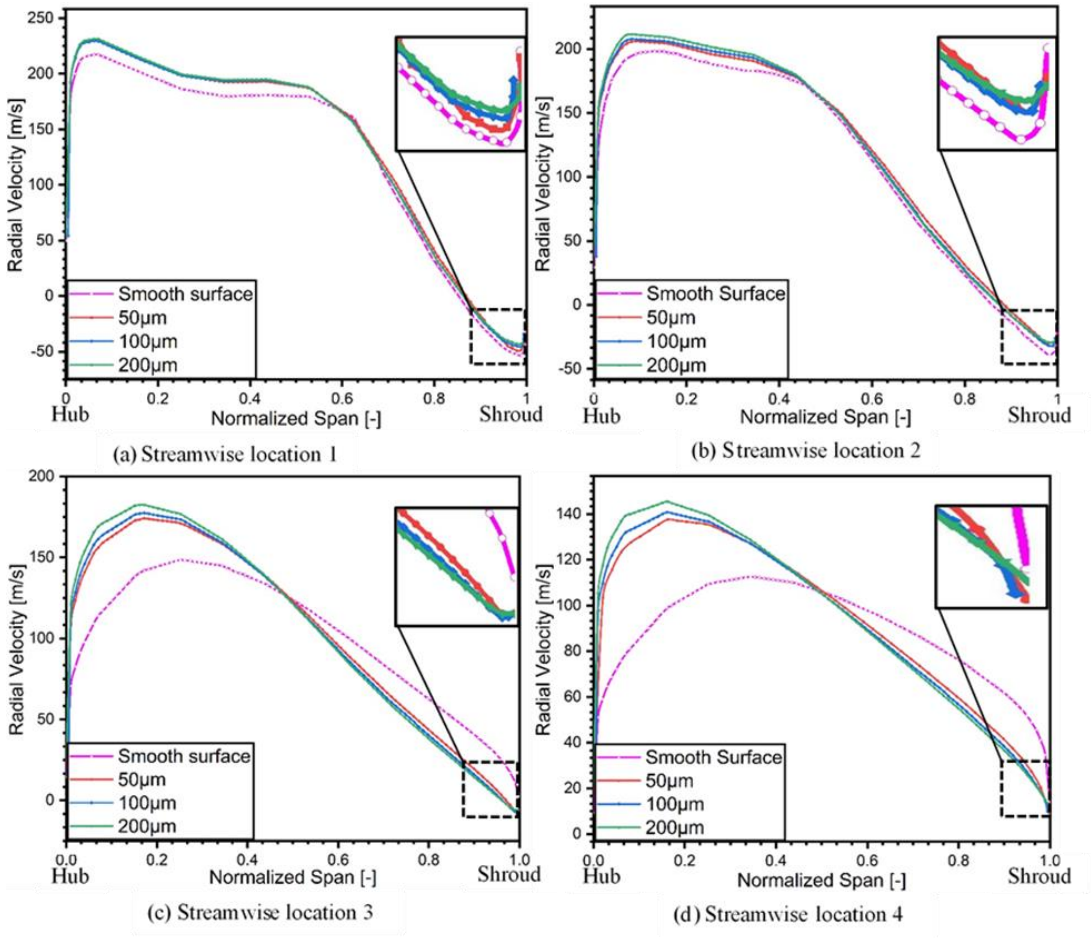

Figure 26: Radial velocity in the diffuser section at 4 streamwise locations

It is shown in Fig. 27 at different streamwise locations along the diffuser's meridional plane tangential velocity has been distributed spanwise at four different locations. It is evident from Fig. 23 that an increase in surface roughness greatly affects the tangential velocity of the compressor. It is noted that on each streamwise location there is a great reduction in the tangential velocity of the compressor, which results in the overall performance reduction of the turbomachine (i.e. Centrifugal compressor). This decrease in the tangential velocity is due to a drop in the frictional losses, which counterweighs for the decline in the performance [2].

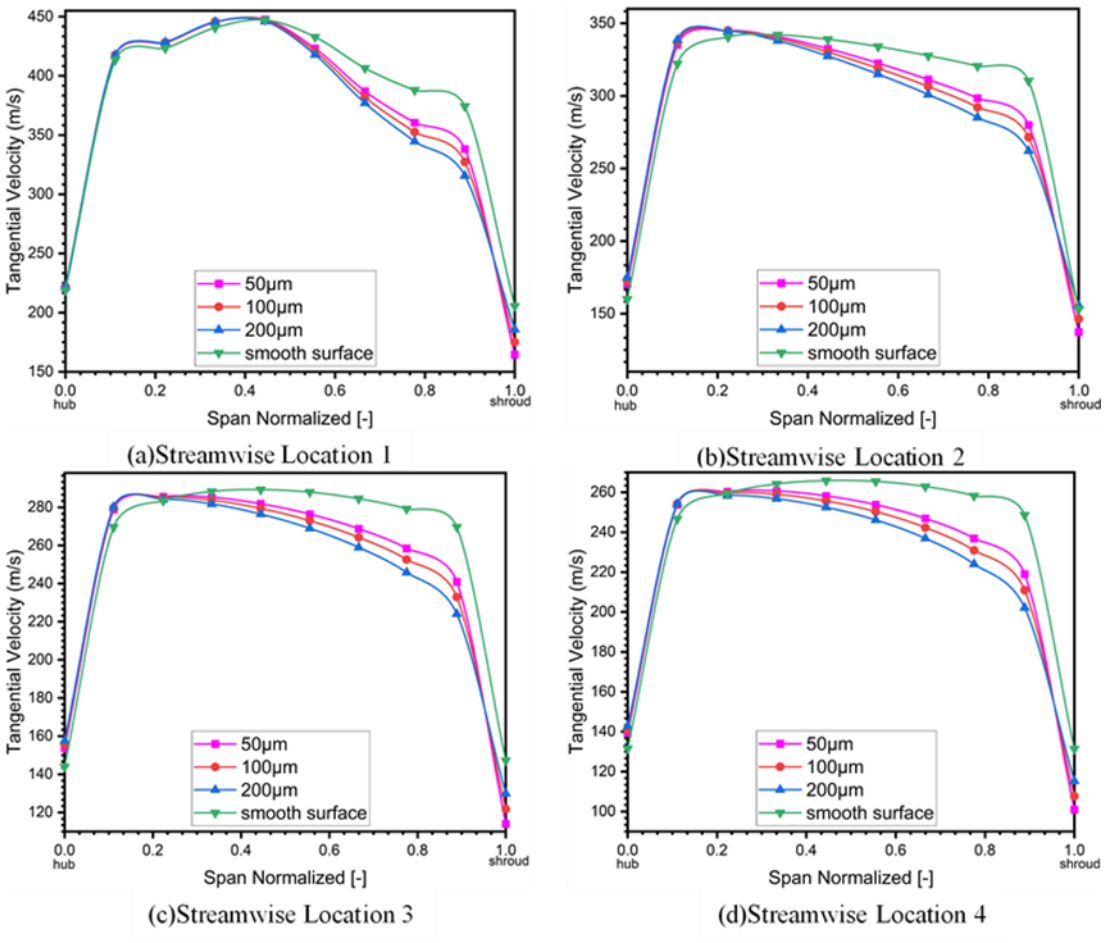

Figure 27: Tangential velocity in diffuser section at 4 streamwise locations

Chapter 5

Conclusion and Recommendations

5.1 Conclusion

Being the essential part of turbocharger for automotive applications, the CFX module of ANSYS has been used to execute centrifugal compressor flow and performance analysis. To perform numerical simulations, First the transition models (k-ε) and (k-ω SST) turbulence models existing in the CFX module (ANSYS) have been used to study the flow field and measure the performance parameters for performance Speedline at the constant rotational speed of 50,000 rpm. In the second part of the analysis, this work concentrates on the influence of different roughness magnitudes on the performance, operating range, stall margin, and flow stabilization of centrifugal compressor.

Comprehensive performance analysis of the baseline SRV2-O compressor designed and developed by DLR (German Aerospace Center) has been executed using the CFD tools. The compressor has been 3D modeled in the BladeGen module of ANSYS, Grid independence has been performed in the TurboGrid module and then performance analysis is carried out in ANSYS-CFX. To study the first part, numerical simulations have been performed to validate the experimental data by comparing it with numerical simulations results. It is concluded from the current research that:

- The k-ε and k-ω SST turbulence model overpredicted the experimental data by 8% and 2.3% respectively. This deviation from the experimental data is because of the limitations of each turbulence model, as the k-ε model better studies the planar shear layer and k-ω SST turbulence model shows more realistic results for viscous sublayer
- The aerodynamics analysis is carried out for the baseline SRV2-O compressor at the highest efficiency or design point. It demonstrates the low relative Mach number locations on the diffuser shroud, which start at the diffuser inlet and

then grow along with diffuser shroud. This region appears at a low mass flow rate causing flow separation and flow reversal and is called stall phenomena

- The choke point is limited by a high mass flow rate, which is caused by the throttle area between the main and splitter blade
- At low mass flow rate, the maximum loss production is attributed to the static entropy generation at the diffuser shroud, which occurs as a result of recirculating flow. All these recirculation flows and flow separations indicate the flow instabilities in the centrifugal compressor
- Because of engineered surface roughness ranging 50-200 μm on the diffuser shroud, flow reversal and flow separation near the diffuser shroud is completely eliminated
- The percentage drop in pressure ratio at stall point for 50 μm is 3.3 %, 4.2 % for 100 μm and 5.08 % for 200 μm using the k-ω SST turbulence model
- The percentage drop in pressure ratio at the stall point for 50 μm is 3.1 %, 3.3 % for 100 μm and 3.5 % for 200 μm using the k-ε model

5.2 Recommendations and Future Work

The current steady-state analysis showed effective results as the flow instabilities i.e. flow recirculation and flow separation has been reduced because of the application of surface roughness on diffuser shroud of centrifugal compressor and hence claim further examination. As the flow field in the centrifugal compressor is unsteady, more precise results can be obtained if time-dependent simulations are performed. It is recommended for future work to carry out time-dependent simulations for the most realistic improvement in the stability range. It is also recommended to apply other passive flow control methods to reduce flow instability such as vortex generators and creating cavity on diffuser shroud for steady and unsteady simulations.

References

[1] G. Eisenlohr *et al.*, “Gt-2002-30394 Investigations of the Flow Through a High,” pp. 1–9, 2002.

[2] P. Kapoor, “Influence of Surface Roughness on Flow Instabilities in a Centrifugal Compressor,” pp. 1–24.

[3] X. Zheng, Z. Sun, T. Kawakubo, and H. Tamaki, “Experimental investigation of surge and stall in a turbocharger centrifugal compressor with a vaned diffuser,” *Exp. Therm. Fluid Sci.*, vol. 82, pp. 493–506, 2017.

[4] A. P. Heffron, “Rotating Stall and Passive Flow Control on Blade Profiles and in Centrifugal Compressors,” 2017.

[5] X. Xue, T. Wang, T. Zhang, and B. Yang, “Mechanism of stall and surge in a centrifugal compressor with a variable vaned diffuser,” *Chinese J. Aeronaut.*, vol. 31, no. 6, pp. 1222–1231, 2018.

[6] T. R. Camp and I. J. Day, “1997 Best Paper Award—Turbomachinery Committee: A Study of Spike and Modal Stall Phenomena in a Low-Speed Axial Compressor,” *J. Turbomach.*, vol. 120, no. 3, pp. 393–401, 1998.

[7] I. J. Day, “Stall Inception in AxiakJFIow Compressors,” vol. 1, no. January 1993, pp. 1–9, 2014.

[8] K. Brun and R. Kurz, “Analysis of Secondary Flows in Centrifugal Impellers,” *Int. J. Rotating Mach.*, vol. 2005, no. 1, pp. 45–52, 2005.

[9] N. D. Katopodes, *Geophysical Effects*. 2019.

[10] R. J. Zhao *et al.*, “Effect of attack angle on flow characteristic of centrifugal fan,” 2016.

[11] X. Zheng and A. Liu, “Phenomenon and mechanism of two-regime-surge in a centrifugal compressor,” *J. Turbomach.*, vol. 137, no. 8, pp. 1–7, 2015.

[12] F. Tosto, “Master of Science in Vehicle Engineering Master ’ s Thesis in Fluid

Dynamics Investigation of performance and surge behavior of centrifugal compressors through CFD simulations," no. March, 2018.

[13] Y. Bousquet, X. Carbonneau, G. Dufour, N. Binder, and I. Trebinjac, "Analysis of the unsteady flow field in a centrifugal compressor from peak efficiency to near stall with full-annulus simulations," *Int. J. Rotating Mach.*, vol. 2014, 2014.

[14] X. Zheng, Z. Sun, T. Kawakubo, and H. Tamaki, "Experimental investigation of surge and stall in a turbocharger centrifugal compressor with a vaned diffuser," *Exp. Therm. Fluid Sci.*, vol. 82, no. November 2019, pp. 493–506, 2017.

[15] M. R. Feulner, G. J. Hendricks, and J. D. Paduano, "Modeling for control of rotating stall in high speed multi-stage axial compressors," *Proc. ASME Turbo Expo*, vol. 5, 1994.

[16] C. Yang, W. Wang, H. Zhang, C. Yang, and Y. Li, "CO," *Aerosp. Sci. Technol.*, vol. 1, pp. 1–12, 2018.

[17] M. Kita, S. Iwamoto, D. Kiuchi, and R. Kawashita, "PREDICTION OF SUBSYNCHRONOUS ROTOR VIBRATION AMPLITUDE CAUSED BY ROTATING STALL."

[18] E. M. Greitzer, "Surge and Rotating Stall in Axial Flow Compressors - 1, 2.," *Am. Soc. Mech. Eng.*, no. 75-NaN-9, pp. 190–198, 1975.

[19] J. T. Gravdahl, "Modeling and control of surge and rotating stall in compressors," *Sci. Technol.*, p. 141, 1998.

[20] R. A. Strub and M. Sterkrade, "DISCUSSION The paper by Dr . Simon and Mr . Biilsk â€™ amper mentions a working group of the ICAAMC investigating ' Workshop Performance Tests on Turbocompressors .' This discussion provides some supplementary information about the work of this group . In 1," vol. 106, no. April, pp. 499–501, 1984.

[21] M. H. Industries, "Development of a Wide-Range Centrifugal Compressor for

Automotive Turbochargers," vol. 49, no. 1, pp. 68–73, 2012.

[22] X. He and X. Zheng, "Flow instability evolution in high pressure ratio centrifugal compressor with vaned di ff user," *Exp. Therm. Fluid Sci.*, vol. 98, no. July, pp. 719–730, 2018.

[23] R. E. Mayle, "The Role of Laminar-Turbulent Transition in Gas Turbine Engines," 2017.

[24] B. K. Hodge and R. P. Taylor, "A Re-Evaluation of Schlichting â€™ s Surface Roughness Experiment o," vol. 106, no. March 1984, pp. 60–65, 2016.

[25] J. P. Bons, "A Review of Surface Roughness Effects in Gas Turbines," vol. 132, no. April 2010, pp. 1–16, 2013.

[26] G. Eisenlohr, P. Dalbert, H. Krain, H. Pröll, F.-A. Richter, and K.-H. Rohne, "Analysis of the Transonic Flow at the Inlet of a High Pressure Ratio Centrifugal Impeller," p. V001T01A007, 2014.

[27] M. Engineering, "Modeling curvature effects on turbulence for turbomachinery flows Roberto Suarez Raspopov."

[28] P. Jonáš, O. Hladík, O. Mazur, and V. Uruba, "By-pass transition of flat plate boundary layers on the surfaces near the limit of admissible roughness," *J. Phys. Conf. Ser.*, vol. 318, no. SECTION 3, 2011.

[29] A. Stein, "COMPUTATIONAL ANALYSIS OF STALL AND SEPARATION CONTROL by," no. May, 2000.

[30] T. Reports, *Flow instabilities in centrifugal compressors at low mass fl ow rate by Elias Sundstr ¨*, no. December. 2017.

[31] M. M. U. Rehman, T. A. Cheema, F. Ahmad, M. Khan, and A. Abbas, "Thermodynamic Assessment of Microchannel Heat Sinks with Novel Sidewall Ribs," pp. 1–12, 1981.

[32] F. R. Menter, "Two-Equation Eddy-Viscosity Turbulence Models for Engineering Applications," vol. 32, no. 8, 1994.

[33] Ansys, “ANSYS ICEM CFD User Manual,” *Knowl. Creat. Diffus. Util.*, vol. 15317, no. October, pp. 724–746, 2016.

[34] A. Confidential, “Lecture Theme,” 2014.

[35] R. Placek and P. Ruchała, “The flow separation development analysis in subsonic and transonic flow regime of the laminar airfoil,” *Transp. Res. Procedia*, vol. 29, pp. 323–329, 2018.

[36] Q. Xiao, W. Liu, and A. Incecik, “Flow control for VATT by fixed and oscillating flap,” *Renew. Energy*, vol. 51, pp. 141–152, 2013.

[37] J. Zhong, J. Li, P. Guo, and Y. Wang, “Dynamic stall control on a vertical axis wind turbine aerofoil using leading-edge rod,” *Energy*, vol. 174, pp. 246–260, 2019.

[38] R. Urbina, B. P. Epps, M. L. Peterson, and R. W. Kimball, “A dynamic stall model for analysis of cross-flow turbines using discrete vortex methods,” *Renew. Energy*, vol. 130, pp. 1130–1145, 2019.

[39] L. Guoqiang, Z. Weiguo, J. Yubiao, and Y. Pengyu, “Experimental investigation of dynamic stall flow control for wind turbine airfoils using a plasma actuator,” *Energy*, vol. 185, pp. 90–101, 2019.

[40] K. AL-JABURI, D. FESZTY, and F. NITZSCHE, “A methodology for simulating 2D shock-induced dynamic stall at flight test-based fluctuating freestream,” *Chinese J. Aeronaut.*, 2019.

[41] H. F. Müller-Vahl, C. N. Nayeri, C. O. Paschereit, and D. Greenblatt, “Dynamic stall control via adaptive blowing,” *Renew. Energy*, vol. 97, pp. 47–64, 2016.

[42] J. Yen and N. A. Ahmed, “Enhancing vertical axis wind turbine by dynamic stall control using synthetic jets,” *J. Wind Eng. Ind. Aerodyn.*, vol. 114, pp. 12–17, 2013.

[43] A. Bianchini, F. Balduzzi, G. Ferrara, and L. Ferrari, “Critical Analysis of Dynamic Stall Models in Low-Order Simulation Models for Vertical-Axis

Wind Turbines," *Energy Procedia*, vol. 101, no. September, pp. 488–495, 2016.

[44] A. Meana-Fernández, I. Solís-Gallego, J. M. Fernández Oro, K. M. Argüelles Díaz, and S. Velarde-Suárez, "Parametrical evaluation of the aerodynamic performance of vertical axis wind turbines for the proposal of optimized designs," *Energy*, vol. 147, pp. 504–517, 2018.

[45] F. R. Menter, R. B. Langtry, S. R. Likki, Y. B. Suzen, and P. G. Huang, "A Correlation-Based Transition Model Using Local Variables — Part I : Model Formulation," vol. 128, no. July 2006, pp. 413–422, 2014.

[46] "Turbulent Flows - S. B. Pope, Stephen B. Pope - Google Books." [Online]. Available: https://books.google.com.pk/books/about/Turbulent_Flows.html?id=HZsTw9SMx-0C&redir_esc=y. [Accessed: 06-Mar-2020].

[47] S. B. Pope, "Free Shear Flows: Turbulent Flows." Cambridgr University Press, Cambridge, p. 770, 2000.

[48] S. B. Pope, *Turbulent flows*. Cambridge University Press, 2000.

[49] M. W. Pinson and T. Wang, "Effects of leading-edge roughness on fluid flow and heat transfer in the transitional boundary layer over a flat plate," *Int. J. Heat Mass Transf.*, vol. 40, no. 12, pp. 2813–2823, 1997.

[50] I. P. Castro, H. Cheng, and R. Reynolds, "Turbulence over urban-type roughness: Deductions from wind-tunnel measurements," *Boundary-Layer Meteorol.*, vol. 118, no. 1, pp. 109–131, 2006.

[51] A. Javed, "TURBOMACHINERY Compressor Aero-Thermodynamics."

[52] A. Javed and E. Kamphues, "Evaluation of the Influence of Volute Roughness on Turbocharger Compressor Performance From a Manufacturing Perspective," p. V02DT42A040, 2014.

[53] F. Ghigliazza, A. Traverso, M. L. Ferrari, and J. Wingate, "Gt2008-50562," *Asme Gt*, pp. 1–9, 2008.

[54] A. R. Avio, “Aerodesign and Performance Analysis of a Radial Transonic Impeller for a 9 : 1 Pressure Ratio Compressor,” vol. 115, no. July 1993, pp. 573–581, 2017.

[55] R. Hunziker, H. P. Dickmann, and R. Emmrich, “Numerical and experimental investigation of a centrifugal compressor with an inducer casing bleed system,” *Proc. Inst. Mech. Eng. Part A J. Power Energy*, vol. 215, no. 6, pp. 783–791, 2001.

[56] B. Semlitsch and M. Mihăescu, “Flow phenomena leading to surge in a centrifugal compressor,” *Energy*, vol. 103, pp. 572–587, 2016.

[57] Y. SENOO and M. ISHIDA, “Deterioration of compressor performance due to tip clearance of centrifugal impellers.,” *Trans. Japan Soc. Mech. Eng. Ser. B*, vol. 52, no. 473, pp. 386–392, 2011.

[58] . S. M. S., “Effect of Tip Clearance on Performance of a Centrifugal Compressor,” *Int. J. Res. Eng. Technol.*, vol. 2, no. 9, pp. 445–453, 2015.

[59] C. Xu and R. S. Amano, “Effects of Asymmetric Radial Clearance on Performance of a Centrifugal Compressor,” *J. Energy Resour. Technol.*, vol. 140, no. 5, p. 52003, 2017.

[60] C. Kim, H. Lee, J. Yang, C. Son, and Y. Hwang, “Study on the performance of a centrifugal compressor considering running tip clearance,” *Int. J. Refrig.*, vol. 65, pp. 92–102, 2016.

[61] N. Buffaz and I. Trébinjac, “Impact of Tip Clearance Size and Rotation Speed on the Surge Onset in a High Pressure Centrifugal Compressor,” p. 2491, 2013.

[62] A. Jaatinen, T. Turunen-Saaresti, A. Grönman, P. Röyttä, and J. Backman, “Experimental Study of the Effect of the Tip Clearance to the Diffuser Flow Field and Stage Performance of a Centrifugal Compressor,” p. 641, 2013.

[63] S. Mirzaee, X. Zheng, and Y. Lin, “Improvement in the stability of a turbocharger centrifugal compressor by tip leakage control,” *Proc. Inst. Mech. Eng. Part D J. Automob. Eng.*, vol. 231, no. 5, pp. 700–714, 2017.

[64] S. N. Danish, Chaochen Ma, and Y. Ce, “The influence of tip clearance on centrifugal compressor stage of a turbocharger,” *Proc. 4th WSEAS Int. Conf. Fluid Mech. Aerodyn. Elounda, Greece*, vol. 2006, pp. 6–11, 2006.

Performance Variation of Transonic Centrifugal Compressor at Different Tip Clearances Using Numerical Simulations

Amjid Khan[1*], Adeel Javed[2]
Center for Advanced Studies in Energy
National University of Sciences and Technology H-12 Islamabad, Pakistan
*17teeamjid@uspcase.nust.edu.pk, adeeljaved@uspcase.nust.edu.pk

***Abstract*— One of the prime contributors to entropy generation and performance loss in centrifugal compressors is the presence of tip-clearance gap and associated tip-leakage flow. This paper aims to study the fundamental performance variation of a high-pressure transonic centrifugal compressor at different tip clearances using three-dimensional (3D) numerical simulations. In this study the test case used is the transonic SRV2-O compressor designed and developed by DLR (German Aerospace Center). Reynolds Averaged Navier-Stokes (RANS) based k-ε model has been used for numerical simulations. The performance of centrifugal compressor is significantly affected by tip-leakage flow, which combines with the secondary flow and results in a considerable entropy generation accumulated at the shroud suction-side of the impeller blade. For understanding of flow mechanism, eleven different tip clearances have been simulated along with comprehensive evaluation of the tip-leakage flow. At constant tip-clearance ranging 0.01 to 1mm, a loss of about 17.7% occurred in the stage pressure ratio of compressor and isentropic efficiency was dropped by 5.5%, at design conditions of 2.55 kg/s of mass flow rate and 50,000 1/min. The compressor isentropic efficiency and pressure ratio is observed optimum at constant tip-clearance in range 0.09 mm and 0.18 mm. While at variable tip-clearance between leading-edge (LE) and trailing-edge (TE), almost 11 percent loss has been noted in the stage pressure ratio, while isentropic efficiency was reduced by 3.3 percent as tip clearance increased from 0.3 to 1.1mm at the leading edge and 0.1 to 0.9 mm at the blade exit of the impeller. This paper provides the quantitative estimate of losses in compressor pressure ratio and efficiency due to tip-clearance.**

Keywords—Centrifugal compressor, Tip-clearance, Numerical simulations, Entropy, Transonic, High pressure

14 INTRODUCTION

High pressure centrifugal compressors are broadly used in automotive turbochargers and micro gas turbines. Usually, unshrouded impellers are used for these applications with splitter blades. So therefore, the performance is retrograded by pressure loss because of tip-clearance between shroud casing and blade tip of impeller. To circumvent huge stresses with rise in weight, unshrouded compressors are used [57]–[64]. It has been experimentally analysed that with small tip clearance, unshrouded impeller performance was better than shrouded impeller with similar design in a larger flow range except at larger flow rate [2]. Even though the design and manufacturing of the centrifugal compressor have been successful but still there is a need of research to study tip leakage flow effect mandatory to understand losses and refine performance.

One of the most dominant factors to entropy generation and losses in centrifugal compressor is the presence of tip-clearance gap and corresponding tip-leakage flow. Tip-clearance is leakage occurs between tip of impeller blade and stationary volute casing. Centrifugal compressor inhabits large flow path for the flow, so these losses are more detrimental in centrifugal compressor as compared to axial compressor [3]. The flow pattern becomes too complex when tip leakage flow and blade vortex flow interact with each other [4].

Number of numerical simulations and experiments have been executed to study effects of tip-leakage flow on pressure ratio and efficiency of centrifugal compressor. Experimental investigation showed that As tip-clearance is slightly increased from design point, a reduction in the static pressure rise of compressor and operating range has been noted, the numerical simulations showed the same result as shown in fig. 8 [5]. Experimental examination experienced 4 percent drop in compressor efficiency as tip-clearance was raised from 0.0125 to 0.125mm, so it was concluded that greater tip-clearance, larger is drop in the compressor efficiency [6,7]. A drop of 15% in the stage pressure has been calculated by numerical simulations as tip-clearance is raised from 0mm to 1mm at design mass flowrate of 0.35kg/s. The stage efficiency is noted optimum at constant tip-clearance in range 0.1mm-0.2mm [1]

The measured and simulated results showed that drop in efficiency of transonic flow high pressure-ratio compressor is smaller than low pressure-ratio compressors, if at exit of impeller tip-clearances are equal [2]. Flow obstruction near shroud and slip velocity at impeller exit is usually caused by tip-leakage flow effects pressure ratio drop and generate entropy [3]. With increase of tip-clearance, choke shifts to high mass flow rate [8]. The efficiency drop is higher at higher mass flow rates due to enlarged tip-clearance [7].

The tip-clearance jet and vortex create huge mean velocity gradients that create vorticity and turbulent kinetic energy, and these velocity changes are main loss sources in axial compressors. It is reasonable, that the main cause for the tip-clearance losses are same for both axial and centrifugal compressors [9]. As centrifugal compressor is considered to be adiabatic, so the main loss in efficiency occurs is because of entropy generation by irreversibilities. In the turbulent boundary layer, the entropy creation occurs within laminar sublayer. The diffuser major losses are because of mixing of passage and blade wakes, and at impeller exit as swirl angle advances, it amplify losses [10].

There are two methods to understand tip-leakage mechanism and its effect on pressure ratio and efficiency of

centrifugal compressor, first by keeping the blade height constant and varying the shroud and second keeping shroud constant and varying the blade height. In this paper numerical simulations have been carried out to examine effect of constant and variable tip-clearances by keeping blade height constant. Variable tip-clearance means different values of tip-clearance at leading and trailing edge of blade. Till now, most of work had been executed on constant tip clearance, while in this paper the newest work is the effect of variable tip-clearance. The compressor is evaluated for eleven constant tip-clearance levels from 0.01 to 1mm and variable tip-clearance levels from 0.3,0.1mm to 0.6,0.8mm at design conditions; mass flow rate 2.55kg/s and 50,000rpm. In variable tip-clearance, first value represents tip-clearance at leading edge of blade and second value represent at trailing edge of blade. The order of paper is in this pattern; First of all, specification of test case is tabulated. Then numerical setup has been explained and then validation results and results of ANSYS-CFX are discussed and concluded.

15 SPECIFICATIONS OF SIMULATED CASE

A centrifugal compressor test has been studied to understand effect of tip-clearance having high pressure ratio, mass flow coefficient and specific speed. The test case was designed and built by DLR (German Aerospace Centre).

As shown in the Fig. 1, impeller with13 full and 13 splitter blades. Splitter blades leading edges is at 26% of full blade chord. The exit diameter of test case compressor is 112mm and nominal tip speed is 586m/s at 50000 1/min. A vaneless diffuser is connected after the impeller [1].

The compressor (SRV2-O) test case data is shown in table 1:

TABLE 3: SPECIFICATION OF SRV2-O COMPRESSOR [1]

Parameter	**Value**	**Unit**
Inlet ambient pressure, P_{t1}	101325	[Pa]
Inlet ambient temperature, T_{t1}	288.15	[K]
Design Shaft rotation, n	50000	[1/min]
Design mass flowrate, m	2.55	[kg/s]
Number of full/splitter blades	13/13	-
Tip speed of Impeller	586	[m/s]
Pressure ratio of Impeller	6.1	-
Impeller efficiency	84%	-

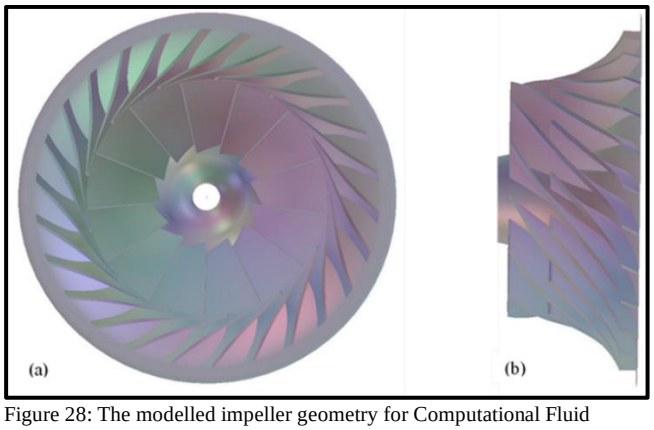

Figure 28: The modelled impeller geometry for Computational Fluid Dynamics analysis (a)Front View (b)Side View

16 NUMERICAL SETUP

17 Turbulence Model

The first step is to model 3D geometry for compressor. Based on available test case data, 2D blade shape has been modified to 3D model using Commercial modeler ANSYS BladeGen. Only single passage of impeller having single pair of blades (full and splitter) has been modeled to reduce computational time for simulation due to smaller number of mesh elements as shown in Fig. 3. For CFD simulations ANSYS CFX 15 is used to model flow field for test case (SRV2-O) compressor under steady state conditions. K-epsilon model used as turbulence model as it gives better results for planar shear layer and recirculating flows as is the case of centrifugal compressor. According to the K-epsilon turbulence model criteria, the value of Y-plus is set to 35.

18 Grid Generation (Turbogrid)

After modelling centrifugal compressor in BladeGen, an H-grid mesh topology was created in ANSYS TurboGrid module. TurboGrid is a meshing scheme for turbomachinery configurations, it selects automatic and refined mesh quality for most complex geometries creating structured mesh. For the better mesh quality, compressor computational domain is divided to H-grid topology with splitter blades arrangement. Design tip clearance for this case is variable tip clearance of 0.5,0.3mm. Mesh is generated using H-grid with number of elements at the inlet and outlet 25 each as depicted in Fig. 2. A grid independency test executed using 3 distinct grid sizes for complete compressor. The grid with total number of mesh elements 560788 and total number of nodes 504345, has been found adequate as alteration in pressure ratio and isentropic efficiency was negligible in this range of elements.

19 Computational Solver

In order to study inlet, impeller and diffuser, boundary conditions were specified in CFD model and stage mixing approach is used. The inlet boundary condition of the passage is 1atm pressure and 288.15K temperature. The design mass flow rate of 0.196 kg/s per passage is kept as outlet boundary condition. The residuals were ($1x10^{-5}$) in magnitude for convergence criteria. For convergence, mass flow rate and isentropic efficiency have been monitored.

First order finite volume discretization is used for turbulence numeric and high resolution as advection scheme. The simulations of compressor were performed using commercial ANSYS CFX flow solver. The time scale factor 1 is used for calculations over 1000 iterations for steady state 3D centrifugal compressor analysis.

To analyse tip clearance effect, Reynolds Averaged Navier-Stokes (RANS) equations for K-ε Model has been used as turbulence model for constant and variable tip-clearances simulations.

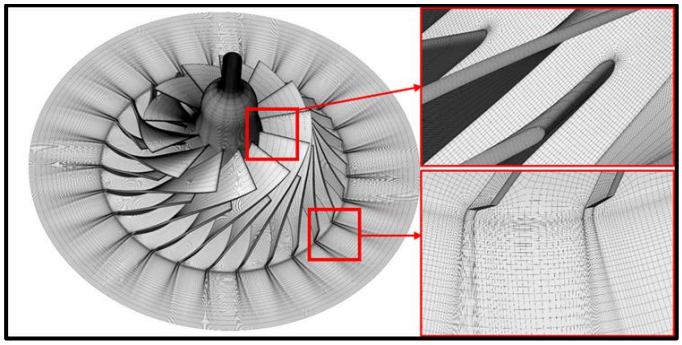

Figure 29: Computational Mesh Domain

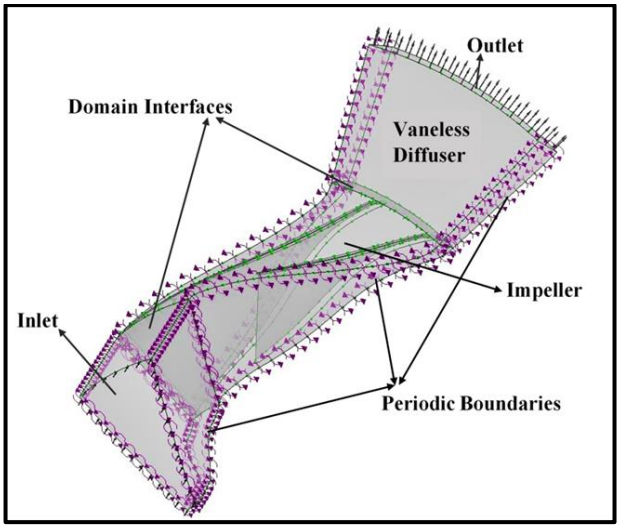

Figure 30: Compressor computational domain

20 RESULTS AND DISCUSSIONS

21 Validation Results and Overall Perfomance

The results of experimental data are validated using ANSYS CFX to check the suitability of this solver. Analysis carried out at design mass flowrate of 2.55kg/s and design speed of 50,000 1/min, this solver over predicted the experimental data by 9% but still better results than other CFD Solvers like VISIUN, FLOWSIM and TASCFLOW[26].

At design mass flowrate, constant and variable tip-clearance sizes were selected for two main reasons. Primarily, to understand effect of tip-clearance on the pressure ratio and efficiency of test case SRV2-O compressor and secondly to choose most optimum size of tip-clearance for efficient design of compressor. Similar to literature[1], the characteristic curves show significant drop in the performance as shown in the Fig. 4. At constant tip-clearance ranging 0.01 to 1mm, a drop of around 17.7% occurred in stage pressure-ratio of compressor and efficiency was dropped by 5.5%, at design conditions; 2.55kg/s of mass flow rate and 50,000rpm as shown in Fig. 5.

For constant tip-clearance, peak in pressure ratio and ratio occurs from 0.1mm to 0.2mm range of tip clearance. While at variable tip clearance, almost 11% loss has been noted in stage pressure ratio and efficiency is reduced by 3.3% as tip-clearance increased from 0.3mm-1.1mm at leading edge and 0.1mm-0.9 mm at trailing edge of impeller blade as shown in Fig. 6. Simulated data show linear fall in peak pressure ratio and isentropic efficiency as tip-clearance is increases from lower to higher values, but variable tip-clearance showed better results in comparison with constant tip-clearance as drop in overall performance is small in this case.

In variable tip-clearance 0.3,0.1mm, first value 0.3mm represent tip-clearance at leading edge of blade and second value 0.1mm represent tip-clearance at trailing edge.

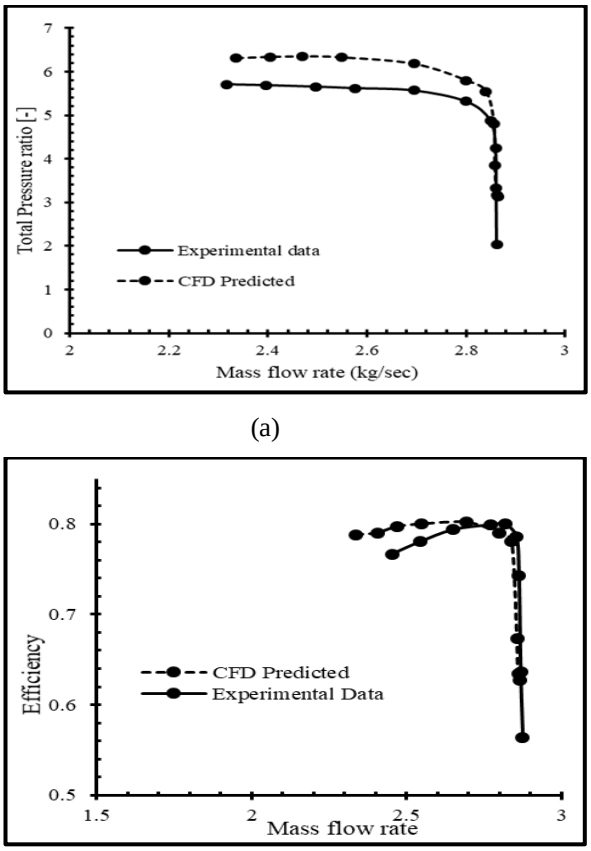

(a)

(b)

Figure 31: Validation of Experimental results (a) Total Pressure Ratio (b) Efficiency

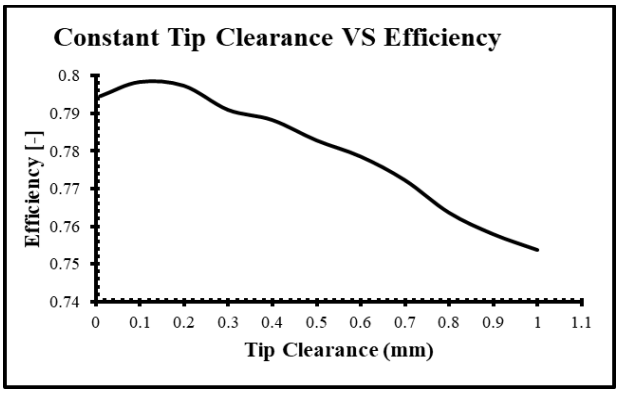

(a)

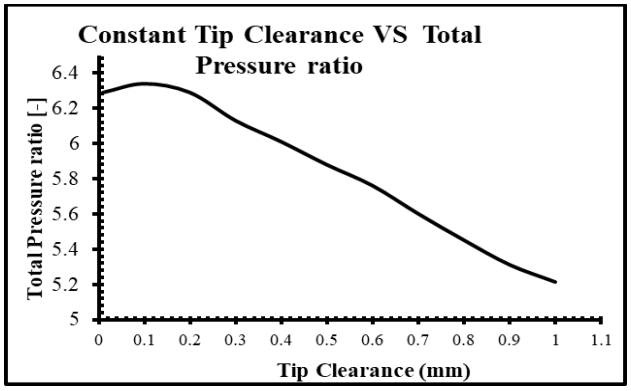

(b)

Figure 32: Constant Tip Clearance (a) Efficiency (b) Pressure Ratio

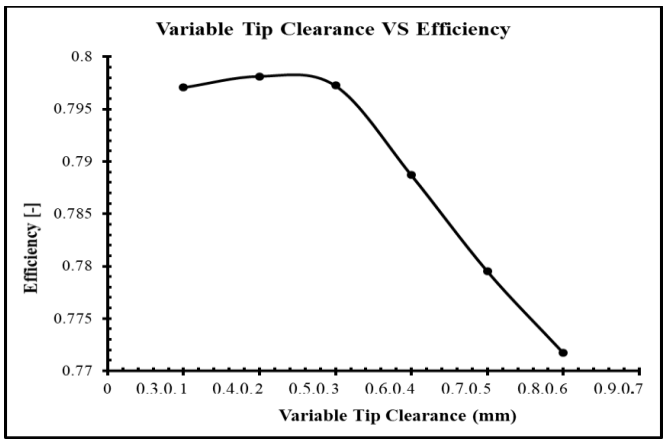

(c)

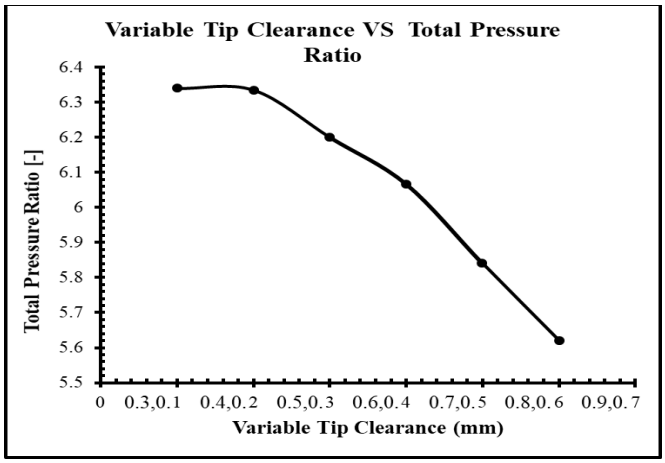

(d)

Figure 33: Variable Tip Clearance (c)Pressure Ratio (d)Efficiency

22 Secondary Flow Streamlines

To understand mechanism of secondary Flow pattern, it is necessary to understand flow streamlines entering blades leading and trailing edge as illustrated in Fig. 7. These flows create vortex, which is extremely unacceptable because these flows cause non uniformity, slip, head losses and implicitly leads to flow separation and stall. To get rid of these flows, splitter blades are installed in the compressor, which control these vortices as depicted in Fig. 7a. The tip-leakage flow-field combines with secondary flow streamlines and alters flow structure at impeller exit. The tip-leakage leaving leading-edge of main blade create tip-leakage vortex and moves to leading-edge of splitter blade. when tip-clearance has been increased, these vortices elongates further and force the flow to separate after the high loss region of impeller exit and cause flow separation and stall phenomena at the outlet diffuser surface, which significantly reduces pressure ratio and efficiency of compressor as depicted in Fig. 7b.

23 Blade Loading

Blade pressure loading for full and splitter blade at constant tip clearance levels 0.1mm, 0.5mm and 1mm and variable tip clearance of 0.3,0.1mm, 0.6,0.4mm and 1,0.8mm respectively at design mass flowrate of 0.196kg/s per passage has been drawn as depicted in Fig. 8. The statistics of pressure is pinched from 1-2 meridional length normalized for pressure and suction side of the compressor blade. A wide

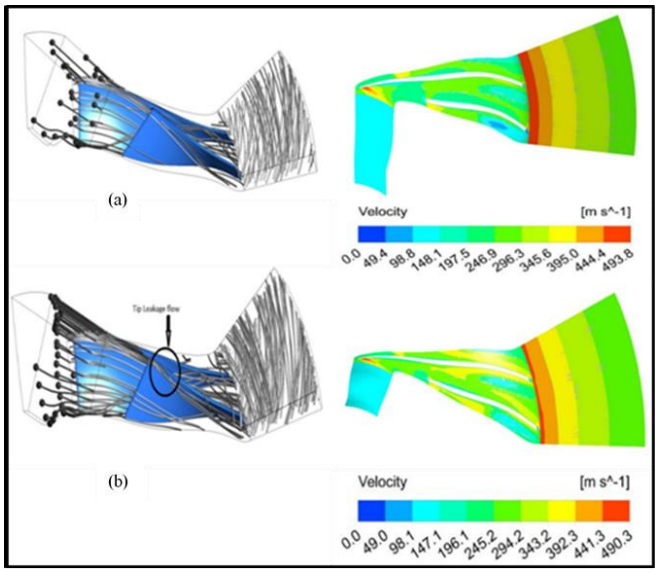

Figure 34: Secondary Flow Streamlines for Constant Tip Clearance (a)0.1mm (b)1mm

range of pressure difference is found between small and large tip-clearance for each blade loading curve. Static pressure rises with small tip-clearance of 0.1mm is 27000Pa and 22000Pa pressure rise with tip-clearance of 1mm has been observed. So, decline in static pressure rise with the rise in tip-clearance is conspicuous from the Fig. 8a and 8b. Same behavior is observed in case of variable tip-clearance as well.

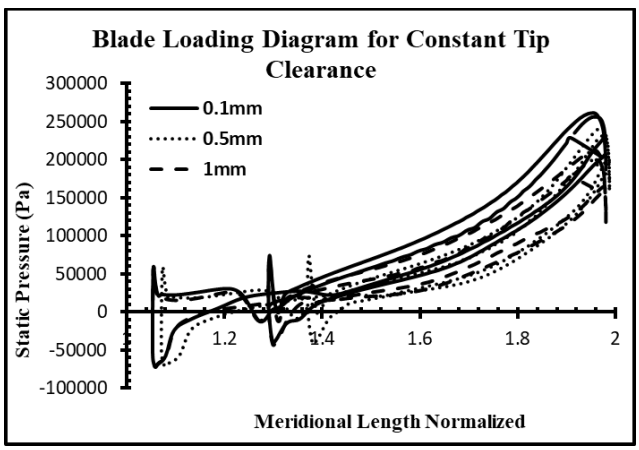

(a)

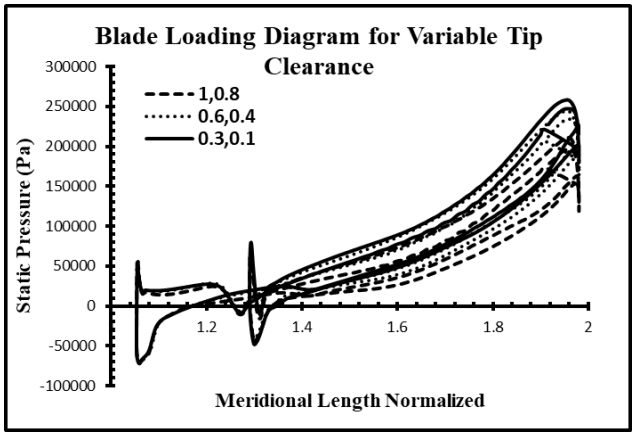

(b)

Figure 35: Blade Loading Diagram at 3 different tip clearances (a)Constant Tip Clearance (b)Variable Tip Clearance

24 Entropy

Static entropy dispersal from inlet to outlet of compressor stage at design mass flowrate of 2.55kg/s; for constant and variable tip clearance is illustrated in the Fig. 9. Static entropy rises steadily from 0.1mm gap to 1mm gap for constant tip clearance due to frictional losses and mixing of flow connected with the dissipation of kinetic energy and shear loss at shroud of the diffuser as clearly shown in Fig. 9. Higher entropy loss is found at all tip clearance levels except the least tip clearance, where it reveals maximum efficiency and total pressure ratio. The maximum cluster of entropy generation is found to at the exit of the impeller of the compressor as shown in Fig. 10.

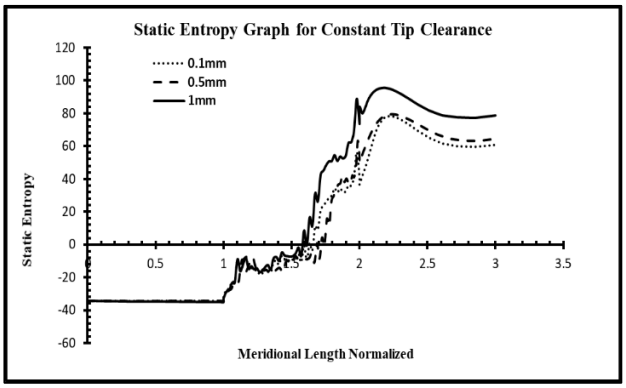

(a)

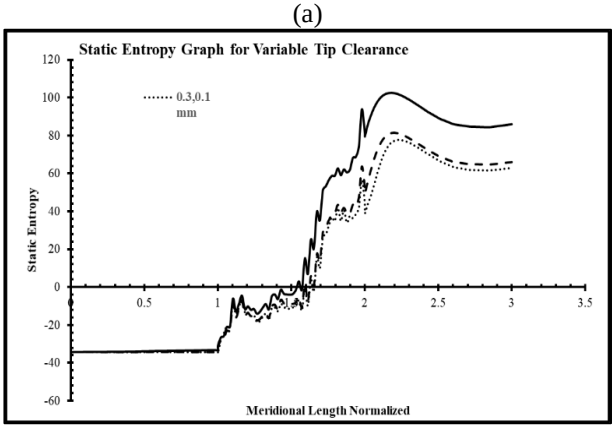

(b)

Figure 36: Entropy Generation from Inlet to Outlet at design mass flow rate of 2.54kg/sec (a) Constant Tip clearance (b) Variable tip Clearance

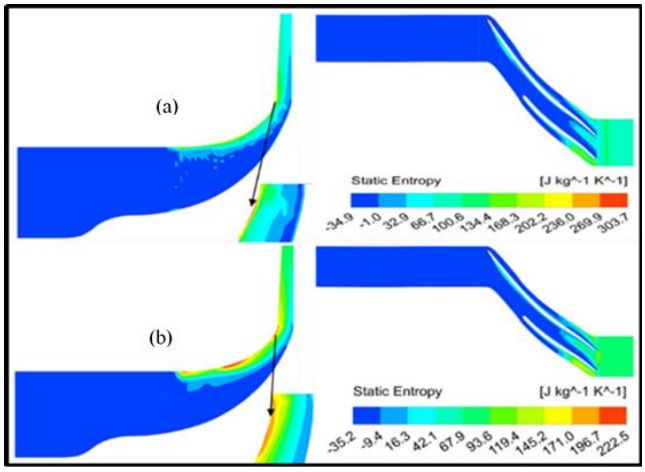

Figure 37: Entropy Generation Contours from Inlet to Outlet for tip clearance (a)0.1mm (b)1mm

25 CONCLUSIONS

The comprehensive study of tip-clearance conferred in this paper has revealed the numerical statistics to evaluate the impact of tip-clearance on overall performance and flow characteristics of test case centrifugal compressor for turbocharger applications. At different tip-clearances for two cases: constant and variable tip clearance have been investigated and the following deductions can be obtained from assessment:

- At constant tip-clearance ranging 0.01mm-1mm, a drop of 17.7% occurred in stage pressure ratio of compressor and isentropic efficiency was dropped by 5.5%, at design conditions of 2.55 kg/s of mass flow rate and 50,000 1/min. The compressor isentropic efficiency and pressure ratio is optimum in range 0.09mm and 0.18mm for constant tip-clearance
- At variable tip clearance between leading-edge (LE) and trailing-edge (TE), almost 11 percent loss has been noted in the stage pressure ratio, while isentropic efficiency was reduced by 3.3 percent as tip clearance increased from 0.3 to 1.1mm at the leading edge and 0.1 to 0.9mm at blade exit of impeller
- Tip-leakage flow greatly effects the centrifugal compressor performance, which combines with the secondary flow and results in a considerable entropy generation accumulated at the shroud suction-side of the impeller blade decreasing the efficiency and pressure ratio of the compressor
- Maximum entropy generation occur at the exit of impeller in both cases of constant and variable tip clearance of compressor

ACKNOWLEDGMENT

The authors are acknowledging their gratitude for the support of U.S-Pakistan Centre for Advance Studies in Energy (USPCAS-E) and the United States Agency for International Development (USAID).

REFERENCES

[1] Y. SENOO and M. ISHIDA, "Deterioration of compressor performance due to tip clearance of centrifugal impellers.," *Trans. Japan Soc. Mech. Eng. Ser. B*, vol. 52, no. 473, pp. 386–392, 2011.

[2] . S. M. S., “Effect of Tip Clearance on Performance of a Centrifugal Compressor,” *Int. J. Res. Eng. Technol.*, vol. 2, no. 9, pp. 445–453, 2015.

[3] C. Xu and R. S. Amano, “Effects of Asymmetric Radial Clearance on Performance of a Centrifugal Compressor,” *J. Energy Resour. Technol.*, vol. 140, no. 5, p. 52003, 2017.

[4] C. Kim, H. Lee, J. Yang, C. Son, and Y. Hwang, “Study on the performance of a centrifugal compressor considering running tip clearance,” *Int. J. Refrig.*, vol. 65, pp. 92–102, 2016.

[5] N. Buffaz and I. Trébinjac, “Impact of Tip Clearance Size and Rotation Speed on the Surge Onset in a High Pressure Centrifugal Compressor,” p. 2491, 2013.

[6] A. Jaatinen, T. Turunen-Saaresti, A. Grönman, P. Röyttä, and J. Backman, “Experimental Study of the Effect of the Tip Clearance to the Diffuser Flow Field and Stage Performance of a Centrifugal Compressor,” p. 641, 2013.

[7] S. Mirzaee, X. Zheng, and Y. Lin, “Improvement in the stability of a turbocharger centrifugal compressor by tip leakage control,” *Proc. Inst. Mech. Eng. Part D J. Automob. Eng.*, vol. 231, no. 5, pp. 700–714, 2017.

[8] S. N. Danish, Chaochen Ma, and Y. Ce, “The influence of tip clearance on centrifugal compressor stage of a turbocharger,” *Proc. 4th WSEAS Int. Conf. Fluid Mech. Aerodyn. Elounda, Greece*, vol. 2006, pp. 6–11, 2006.

[9] G. Eisenlohr *et al.*, “Gt-2002-30394 Investigations of the Flow Through a High,” pp. 1–9, 2002.

[10] G. Eisenlohr, P. Dalbert, H. Krain, H. Pröll, F.-A. Richter, and K.-H. Rohne, “Analysis of the Transonic Flow at the Inlet of a High Pressure Ratio Centrifugal Impeller,” p. V001T01A007, 2014.